Solar Energy Materials & Solar Cells 285 (2025) 113506

Contents lists available at ScienceDirect

Solar Energy Materials and Solar Cells

journal homepage: www.elsevier.com/locate/solmat

Innovative refractory concrete for high temperature thermal energy storage

J. Ramon Castro [a], Carolina Santini [b], Gabriel Zsembinszki [a], Saranprabhu Mani Kala [a], Franklin R. Martinez [a], Sara Risco [a], Claudia Fabiani [b], Anna Laura Pisello [b,c], Luisa F. Cabeza [a,*]

[a] GREiA Research Group, University of Lleida, Pere de Cabrera 3, 25001, Lleida, Spain
[b] EAPLAB at CIRIAF – Interuniversity Research Centre, University of Perugia, Via G. Duranti 63, 06125, Perugia, Italy
[c] Department of Engineering, University of Perugia, Via G. Duranti 93, 06125, Perugia, Italy

ARTICLE INFO

Keywords:
Thermal energy storage (TES)
Calcium aluminate cement (CAC)
Refractory concrete (RC)
Solar applications
High temperature
Thermal cycles
Smart material

ABSTRACT

Thermal energy storage (TES) systems play an important role in the management of thermal energy and associated consumption. Furthermore, using TES, combustion of fossil fuels and their associated environmental impacts are avoided. In particular, demand for high temperature energy storage is increasing and research focuses on the development of suitable materials for these applications. A limited number of studies focus on the use of sensible heat storage systems that exploit concrete as a TES under high temperature conditions for concentrating solar power (CSP) plant systems. The main drawback to overcome in concrete TES is the degradation of the concrete after charging and discharging thermal cycles. This study aims to develop a novel concrete formulation designed for high-temperature applications and capable of withstanding thermal cycling. To achieve this, a refractory concrete was conceptualized using calcium aluminate cement (CAC) and refractory aggregates, specifically basalt and chamotte. The formulation also incorporates a heat treatment applied after the cu[[ring period to enhance its performance under extreme thermal conditions. This heat treatment is what allows to transform a CAC concrete, that unites the dispersed material through hydraulic nodes, into a refractory concrete, that unites the dispersed material through its ceramisation. The new concrete formulation was analysed to evaluate its performance before and after 25 thermal cycles. Results show that thermal conductivity and compressive strength after ceramisation have values around 1.7 W/m·K and 52 MPa, respectively. It was also observed that the initial thermal treatment was not necessary, because the ceramisation of the concrete can also be achieved during the thermal cycling process if the correct heating and cooling rates are used. The developed new concrete formulation containing refractory aggregates demonstrated excellent thermo-physical and mechanical properties that make it suitable for high-temperature TES applications (temperatures up to 700 °C).

1. Introduction

Thermal or electrical energy production from renewable sources is essential to safeguard the environment and reduce CO_2 emissions into the atmosphere. An appropriate storage system allows to store energy from renewable sources and then use it when necessary, implementing production efficiency. In particular, research focuses on thermal energy storage (TES) which can be applied in various fields including buildings and industries. TES integration in concentrating solar energy (CSP) plants leads to use the inexhaustible heat source of the sun [1] in a more cost-effective and continuous manner. The CSP dispatchability could be guaranteed by high-performance heat storage materials. Pelay et al. [2] presented a review paper on TES systems that are suitable for CSP plants noting that the use of sensible TES systems for CSP is the most widespread due to the reliability, low cost, easy implementation, and extensive experimental feedback availability. Kunwer et al. [3] analysed various sensible TES systems for CSP applications while the study of Achkari et al. [4] underlines how the use of liquid SHS is the most mature and suitable system in this field. However, the review of Mohan et al. [5] underlines that nitrate salts in CSP systems decompose at approximately 600 °C while the use of storage fluids generates corrosion problems related to their containment. For these reasons nowadays, the challenge is to find materials for sensible heat storage applications in solid media at high temperatures.

* Corresponding author.
E-mail address: luisaf.cabeza@udl.cat (L.F. Cabeza).

https://doi.org/10.1016/j.solmat.2025.113506
Received 21 November 2024; Received in revised form 25 January 2025; Accepted 10 February 2025
Available online 16 February 2025

In particular, concrete emerges as a good material for this type of TES applications [6,7]. Khare et al. [8] found that high temperature concretes, such as the high alumina cement-based materials and alumina–silicate geoploymers, were identified as having potential for sensible TES media as they are cheap composite materials but their thermo–-physical and mechanical properties should be optimised for sensible TES by a suitable choice of aggregates, binders, and additives. For example, Wang et al. [9] studied the thermal performance of concrete for TES with experiments on thermal conductivity and specific heat at high temperatures simulating charge/discharge cycles and concluding that siliceous aggregates generally provide enhanced thermal performance over carbonate aggregate concrete across all temperature ranges. Also, supplemental cementitious materials (fly ash, silica fume and ground granulated blast furnace slag) and fibres (especially steel fibres) provide an improvement on concrete thermal properties while a low water-cement ratio tends to increase concrete thermal conductivity. Martin et al. [10] evaluated the importance of thermal conductivity in energy storage of concrete subjected to charge and discharge thermal cycles between 300 °C and 600 °C. Results reveal a thermal conductivity between 1.2 W/m·K and 2 W/m·K at room temperature for the various compositions. Instead, at high temperatures thermal conductivity depends on the concrete mix and the aggregates. The most significant loss in thermal performance occurs during the drying stage. Beyond 600 °C, the siliceous mix exhibits the largest decline.

About mechanical properties at high temperatures generally, the residual compressive strength and the modulus of elasticity decrease as the temperature increases due to the degradation of the material [11]. Supplementary cementitious materials (SCM) and fibre reinforced concrete can improve mechanical performance. Ma et al. [12] identified the materials currently used for this purpose considering the deterioration of concrete mechanical properties at high temperatures. Calcareous aggregates provide a greater resistance than siliceous aggregates. Adding pulverised fly ash and slag to concrete could increase its strength at high temperature, while adding silica fume would reduce this resistance. Xiao et al. [13] reported an overview on high performance concrete underlining the uncertainty on the concrete spalling that can generates randomly. However, the use of polypropylene fibres are found to be more efficacious in reducing the spalling of HPC than steel fibres. Shi et al. [14] examined the theories, raw materials, and preparation techniques for ultra high-performance concrete with compressive strength higher than 150 MPa. The effects of the exposure to high temperatures on possible cracking induced in high strength concrete were studied by Phan [15] whose results shown the relation between the generation of spalling and the resistance to water vapor transport during heating. Significant reduction in pore pressure in high-strength concrete can be achieved with additions of polypropylene fibres. Instead, there was no clear evidence that the presence of silica fume by itself affects the tendency for explosive spalling.

Another solution to implement mechanical resistance is the use of calcium aluminate cement (CAC) in the concrete formulation [16] which succeeds in maintaining its properties under repeated thermal cycles better than ordinary Portland cement (OPC) as the research of Alonso et al. [17] verified subjecting the samples to seventy-five thermal cycles lasting 24 h between 290 °C and 550 °C. Also, Boquera et al. [18] studied the properties of CAC and OPC with silicocalcareous and steel slag aggregates concrete before and after 10 thermal cycles from 290 °C to 700 °C. The use of CAC and OPC paste as the cementing component with steel slag aggregates, provide a limited concrete cohesion under the thermal cycling profile selected. A possible solution is to add supplementary cementitious materials as partial replacement of cement, ensuring compatibility with steel slag aggregate. Instead, Lau et al. [19] evaluated the improvement in crack resistance once steel fibres are incorporated into the concrete mix design.

Furthermore, other studies analysed the use of refractory materials in concrete. For example, Baradaran et al. [20] carried out an experimental program concerning recycled aggregates produced by crushing refractory bricks in replacement of 0, 25, 50, 75 and 100 % of natural sand on concrete composition. Results demonstrated that concrete with refractory aggregates had a residual resistance that reached double the values of conventional concrete over 800 °C. Fharenoltz et al. [21] evaluated ceramics suitable for extreme environment conditions while Scheinherrová et al. [22] analysed cement with high alumina content and basalt reporting better values once fibres of different sizes are mixed in the compound. The porosity reduction, the improvement of the microstructure and homogeneity of the concrete mix are all parameters that influence the mechanical performance therefore complete studies must also concern the physical structure of the samples as in Boquera et al. tests [18,23–25].

This study seeks to make a significant impact by developing an advanced concrete tailored for high-temperature applications, including critical uses in thermal energy storage for Concentrated Solar Power (CSP) plants and other industrial processes. By integrating calcium aluminate cement (CAC) with refractory aggregates like chamotte and basalt, and applying a solid-state sintering heat treatment, this innovative formulation enhances the material's thermal resilience. The outcome is a durable, high-performance concrete capable of withstanding extreme thermal conditions, contributing to the advancement of sustainable energy solutions and improving the efficiency and lifespan of industrial infrastructures. Once refractory concrete samples were produced, they were subjected to 25 thermal cycles between 290 °C and 700 °C. Then, properties such as apparent density, porosity, thermal conductivity, and compressive strength were studied and compared to the non-treated concrete.

2. Research significance

The mineralogy of molten calcium aluminate cement shows that calcium oxide (CaO) and alumina (Al_2O_3) are the main oxides. Depending on their percentages, they combine to form monocalcium aluminate (CA) as the main active phase. This active phase reacts with water to give calcium aluminate hydrates. The formation of these hydrates in the CAC depends on the ambient temperature and humidity. Calcium aluminate decahydrate (CAH_{10}, where C is CaO; A is Al_2O_3; and H is H_2O) is usually formed at temperatures below 15 °C, which transforms into dicalcium aluminate octahydrate (C_2AH_8) and gibbsite (AH_3) with increasing temperature. However, CAH_{10} and C_2AH_8 are metastable in nature and transform into stable tricalcium aluminate hexahydrate (C_3AH_6) and AH_3, with the release of water at temperatures above 27 °C. This process is known as a conversion reaction and is described in Eq. (1) and Eq. (2). This reaction is inevitable, and its rate depends on temperature and humidity [26].

$$2\ CAH_{10} \rightarrow C_2AH_8 + AH_3 + 9\ H \tag{1}$$

$$3\ C_2AH_8 \rightarrow \begin{matrix} 2\ C_3AH_6 + AH_3 + 9\ H \\ [C = CaO;\ A = Al_2O_3;\ S = SiO_2;\ H = H_2O] \end{matrix} \tag{2}$$

Microstructural instability is related to the reactions that cause the conversion of metastable hydrates into stable, permanent, and dense hydrates. In this conversion process, there is a significant release of crystallization water by the hexagonal hydrates when they convert to cubic ones, which evaporates, giving rise to a loss of mass. In turn, it involves the formation of a porous structure that reduces the adhesion between the aggregate and the cement paste. Consequently, a notable drop in the compressive strength is obtained (called residual resistance), which is around 25 % of the maximum foreseen value.

Water/cement ratios that are as low as possible can guarantee high residual resistance by ensuring a sufficient amount of anhydrous cement that can be hydrated at a delayed rate over time, compensating for the loss of mechanical strength produced by the conversion [27]. But if concrete must undergo thermal cycling processes throughout its useful life, the products formed as a consequence of its hydration will lose free water, and then dissipate the chemically combined water. Above 600 °C

and as the dehydration of the hydrated aluminates progresses, the mechanical properties of the compound will gradually decrease, and the material will begin to deteriorate.

Using molten aluminate cement alone is insufficient to produce refractory concrete; the added aggregates must also possess refractory properties, whether of natural or artificial origin. This research aims to ensure that the finest fractions of the refractory aggregates integrate effectively with the calcium aluminate cement matrix, enhancing the material overall performance under high-temperature conditions. Therefore, the increase in the working temperature is not only the cause of the dehydration of the aluminates, but it also leads to the formation of ceramic bonds similar to refractory bricks. This confers additional mechanical resistance to unshaped refractory concrete. If the dehydration of the hydraulic binders when the working temperature increases is the main reason why the mechanical resistance decreases, reaching minimum values around 650 °C, the objective is that the products of cement dehydration ($CaO.Al_2O_3$ (CA), $CaO.2Al2O_3$ (CA_2) and $12CaO.7Al_2O_3$ ($C_{12}A_7$), among others) react with the finest fractions of the refractory aggregates forming new compounds that report an increase in mechanical resistance. These new products that are formed from 800 to 1000 °C are usually the anorthite $CaO.Al_2O_3.2SiO_2$ (CAS_2) and the gehlenite $2CaO.Al_2O_3.SiO_2$ (C_2AS), being the reason for the ceramic bond through a solid-state sintering process [28].

3. Materials and methods

3.1. Materials

The materials used in the dosage presented in this study include CAC under the trade name ALUMINITE, very fine aggregates, and refractory chamotte and basalt gravels. Each of them is described below.

The cement used in this study is CAC, produced and supplied by Cementos Molins Industrial (Barcelona, Spain) following the EN-14647: 2006 standard. The characteristics of the cement according to the manufacturer are presented in Table 1.

Aluminite is a refractory cement that is characterized by containing 43 % aluminium oxide. Its mineralogical composition is based on calcium aluminates, with calcium monoaluminate being the majority. About 90 % of all its components are smaller than 90 μm and none release lime during hydration. Its composition and granulometric curve led to ceramisation at temperatures of approximately 750 °C, improving its thermodynamic performance.

The aggregates selected for the study were chamotte and basalt because they have a low coefficient of thermal expansion and high resistance (Fig. 1). Chamotte is kaolin calcined at 1400 °C in rotary kilns and then ground and classified using high-frequency sieves to achieve particle sizes from 3 μm to 10 mm. Chamotte is rich in alumina and recommended for monolithic refractories - unshaped refractories. It was supplied by ARCIRESA (Gijón, Spain). Basalt is a volcanic igneous rock that was formed by the rapid cooling of lava when it emerged to the Earth's surface, becoming a very hard rock. It was supplied by Pedrera Can Saboia (Fogars de la Selva, Spain). The characteristics of both aggregates are presented in Table 2 and Table 3, respectively. Four granulometries of chamotte were used: filler (0–0.1 mm), filler (0–1 mm), sand (1–3 mm), and gravel (2–5 mm) with fineness modulus of 1.87, 4.05, 6.38, and 7.06, respectively. Two granulometries of basalt were used: gravel (3–6 mm) and coarse aggregate (6–10 mm) with fineness modulus of 7.23 and 8.32, respectively (Fig. 1).

Table 1
Cement characteristics [29].

Property	Value
Chemical analysis	
Aluminium oxide (Al_2O_3)	43 %
Calcium oxide (CaO)	36.1 %
Iron oxide (Fe_2O_3)	11.4 %
Ferrous oxide (FeO)	4.5 %
Silicon oxide (SiO_2)	2.9 %
Chlorine (Cl^-)	0.01 %
Sulphur (S^{2-})	0.03 %
Sulphur trioxide (SO_3)	0.1 %
Alkali	0.07 %
Physical properties (@ atmospheric pressure)	
Density	3.2 g/cm^3
Specific surface Blaine	3270 cm^2/g
Initial setting time	145 min
Final setting time	165 min
Mechanical properties	
Compressive strength	47.7 MPa (6 h)
Compressive strength	65.2 MPa (1 day)

3.2. Methodology

Special attention was paid to the preparation of the refractory concrete to achieve high homogeneity, defining an appropriate procedure. Since the workability of the concrete is affected by the amount of water absorbed by the fine fraction of the chamotte, 24 h before the preparation of the specimens, the chamotte (2–5 mm) was moistened and air-dried under laboratory conditions (temperature = 21 °C; relative humidity = 49 %). Furthermore, since the surface of the finer aggregate cannot be dried after it is wetted, as is the case with coarse aggregate, the chamotte with granulometries 0–0.1 mm, 0–1 mm, and 1–3 mm was placed inside separate plastic bags for 24 h, prior to use.

First, the laboratory concrete mixer model H0052 from Proeti (Madrid, Spain) was moistened with water. With the concrete mixer rotating, the chamottes with granulometries 0–0.1 mm and 0–1 mm and the CAC were poured for 2 min, achieving a close mixture of both fractions. Next, and without stopping the machine, the chamottes with granulometries 1–3 mm and 3–5 mm were poured, rotating the mixture for 1 min, without adding water. As a previous step, half of the superplasticizer had been diluted in half of the necessary water which was added to the mixture by rotating it for 3 min. Afterwards, the concrete mixer was stopped for 30 s, the rest of the coarse aggregates were poured in and the entire mass was mixed for 1 min. Finally, and without stopping the concrete mixer, the remaining water was poured with the other half of the diluted superplasticizer, rotating it for another 3 min (Fig. 2). With this procedure, a settlement of the concrete was achieved in the Abrams cone test (slump test) of 90 mm, sufficient to fill the moulds.

The fresh concrete was poured into steel moulds and vibrated for 60 s with a Controls 55-C0162/E (Milan, Italy) vibrating needle with a diameter of 25 mm at 12000 vibrations/minute to eliminate trapped air bubbles and ensure maximum compactness of refractory concrete. The specimens were formed for 48 h and then cured in a controlled chamber at a temperature of 20 ± 2 °C and relative humidity of 97 ± 2 % for 28 days.

Once the curing period finished the samples were cut to the dimensions of 50 × 50 × 50 mm^3 in order to obtain an adequate quantity of CAC samples for each test carried out. Part of these samples were subjected to a solid-state sintering heat treatment that allows to transform a CAC-based concrete (called CAC in this paper) into a refractory concrete (called RC). The substantial difference between the two types of concrete is that, while CAC unites the dispersed material through hydraulic bonds, RC unites the dispersed material through its ceramisation [32]. Heat treatment involves reaching the sintering temperature of 825 °C and maintaining it for 3 h (Fig. 3). After that, the samples inside the oven were allowed to cool down to ambient temperature by natural cooling, since no cooling device was used. In this way the micrometric particles of CaO, Al_2O_3, and SiO_2 of the CAC and the chamotte come together due to the phenomenon of diffusion of atoms, giving anorthite and gehlenite [28]. After releasing the water, small spaces remain in the structure that allow the particles to move. The high temperature (excitation energy) increases the diffusion of the particles which leads to their sintering and subsequent formation of a neck. The voids in the materials reduced and the solid state on the contact surface

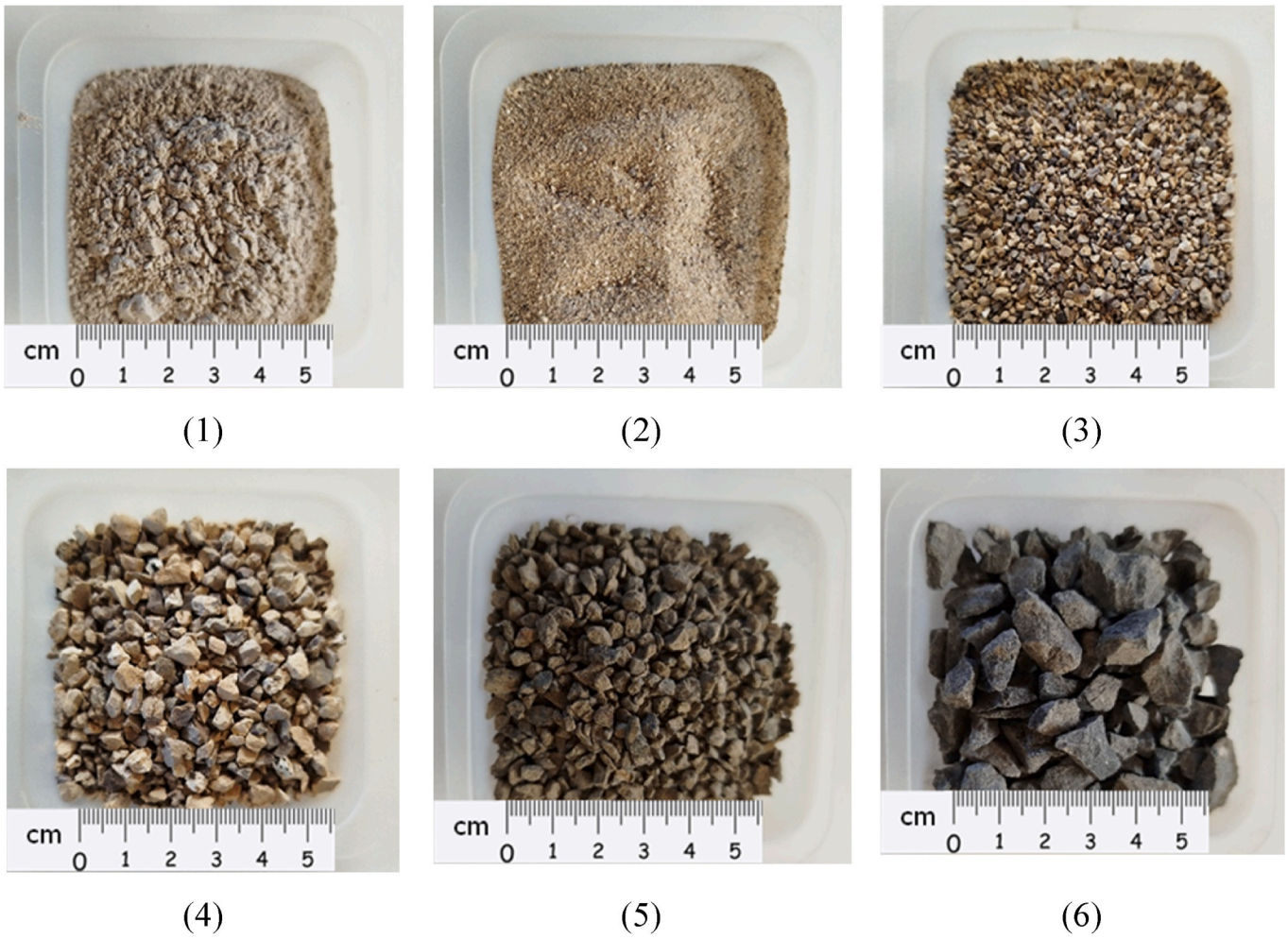

Fig. 1. Photos of all aggregates used: (1) Chamotte (0–0.1 mm), (2) Chamotte (0–1 mm), (3) Chamotte (1–3 mm), (4) Chamotte (2–5 mm), (5) Basalt (3–6 mm), and (6) Basalt (6–10 mm).

Table 2
Chamotte characteristics [30].

Property	Value
Chemical analysis	
Aluminium oxide (Al_2O_3)	43.02 %
Silicon dioxide (SiO_2)	52.13 %
Iron oxide (Fe_2O_3)	1.46 %
Titanium oxide (TiO_2)	2.9 %
Calcium oxide (CaO)	0.15 %
Magnesium oxide (MgO)	0.12 %
Sodium oxide (Na_2O)	0.05 %
Potassium oxide (K_2O)	0.16 %
Physical properties	
Apparent porosity	3 %
Absorption capacity	1.27 %
Bulk density	2.58 g/cm^3

Table 3
Basalt characteristics [31].

Property	Value
Chemical analysis	
Aluminium oxide (Al_2O_3)	14.18 %
Silicon dioxide (SiO_2)	42.6 %
Iron oxide (Fe_2O_3)	5 %
Ferrous oxide (FeO)	6.4 %
Titanium oxide (TiO_2)	2.8 %
Calcium oxide (CaO)	10.39 %
Magnesium oxide (MgO)	0.19 %
Sodium oxide (Na_2O)	3.8 %
Physical properties	
Apparent porosity	0.75 %
Absorption capacity	0.33 %
Bulk density	2.85 g/cm^3

between the particles increases due to the bonding bridges established between particles. As a result, the final compound is more compact and less porous.

Following previous study [18], this research intends to analyse the effects induced by thermal cycles on the new innovative concrete developed. In order to simulate realistic conditions to which the material is potentially subject once used for high temperature applications, samples were placed inside an oven model Naberthem (Germany) set to carry out 25 cycles between 290 °C and 700 °C (Fig. 4). An initial cycle was used to make the temperature go from 290 °C to 700 °C with a low heating rate of 1 K/min. Then, the constant temperature of 700 °C was maintained for 12 h before switching to natural cooling to return to 290 °C. The second cycle is similar to the previous one, but it was repeated for other 24 cycles with a heating rate of 15 K/min between 290 °C and 700 °C. With this approach, one full thermal cycle lasted for about 30 h.

3.3. Analytical methods

The analysis performed on CAC and RC samples aim to evaluate and

Fig. 2. Appearance of fresh concrete and filling of test specimens.

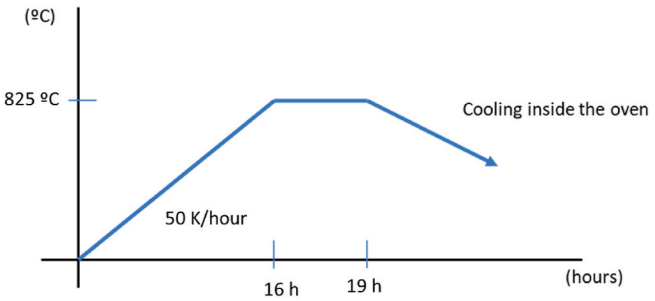

Fig. 3. Temperature profile for the initial heat treatment to obtain RC samples.

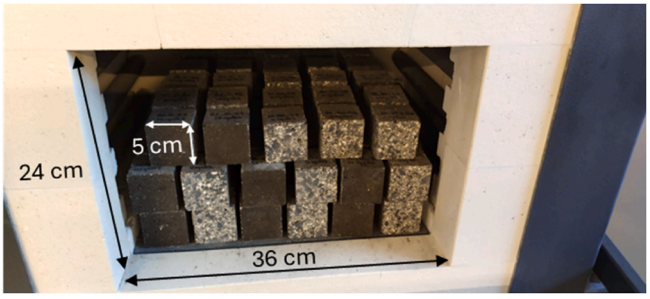

Fig. 4. Samples located in the oven for thermal cycling.

compare the main physical, thermal, and mechanical properties of concrete before and after thermal cycles. First, a visual inspection was conducted to identify possible visible damage before and after 25 cycles compared to the initial samples. Indeed, a high level of degradation cause an alteration of the material properties and indicates poor samples resistance to high temperatures.

About the physical properties, apparent density, weight loss, and open porosity were analysed. Both apparent density and weight loss were evaluated as the average of four different samples of size 50 × 50 × 50 mm^3. In particular, weight loss was calculated using Eq. (3):

$$weight\ loss\ [\%] = \frac{w_{bc} - w_{ac}}{w_{bc}}\ 100 \tag{3}$$

where w_{bc} was the weight of the sample before cycling [g] while w_{ac} was the weight of the sample after cycling [g].

Porosity tests were performed on three samples of size 50 × 50 × 50 mm^3 according to the standard EN 1936:2010 [33] as shown in Fig. 5. The calculation of porosity involved various steps: first samples were dried at 70 °C inside an oven (JP SELECTA Digitronic-TFT 2005163) until the difference between the two weightings at an interval of 24 h is not greater than 0.1 % of the mass of the sample. The dry weight (md) was measured in a scale GRAM model AKA 3200. Then, the samples were introduced in a desiccator to do the vacuum, maintaining the pressure at 2 ± 0.7 KPa for 2 h to remove all the air from the open pores. Later, maintaining the vacuum, water was introduced gradually to the desiccator. Once the samples were totally covered, the vacuum was stopped and maintained the samples in water for 24 h. After this period, the desiccator was opened and the sample was weighed when in contact

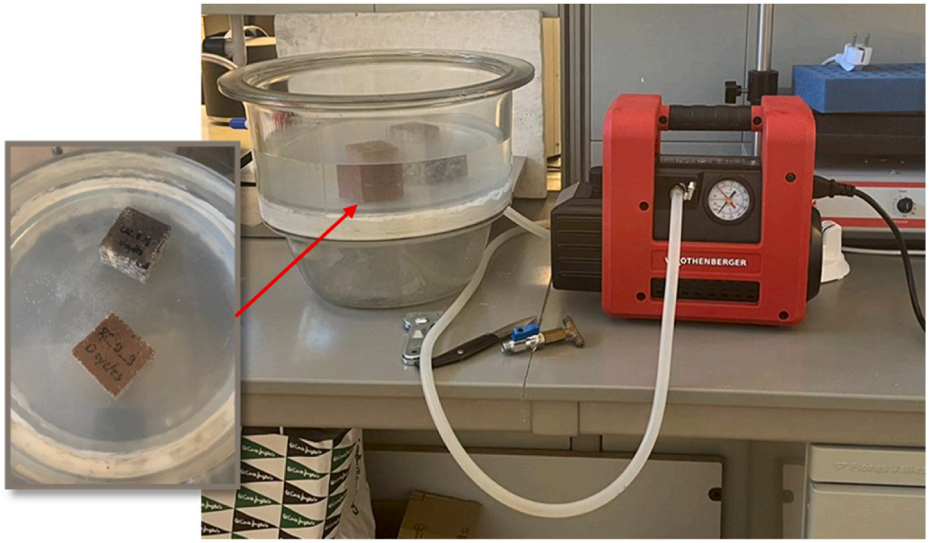

Fig. 5. Porosity measurement setup.

with water, measuring the hydrostatic weight (m_h). Immediately after, the sample was wiped and measured the saturated weight (m_s). Open (P_0) was obtained following Eq. (4):

$$P_0[\%] = \frac{m_s - m_d}{m_s - m_h} 100 \quad (4)$$

Thermal conductivity was carried out on three pairs of concrete samples both for CAC and RC after 0 and 25 thermal cycles. The thermal characterization utilized the Transient Plane Source (TPS) method [34] following the reference standard UNI EN ISO 22007–2:2015 [35]. The experimental setup involved the use of the Hot Disk Kapton sensor n. 8563 for room temperature measurements and of Hot Disk Mica sensor n. 5465 for high temperature measurements. Both sensors were connected to the Hot Disk 2500S and positioned between the flat surfaces of two identical samples. An electric current was passed through it which increases the temperature. By recording the temperature versus time, it is possible to calculate the thermal conductivity of the samples. Thermal conductivity was evaluated at room temperature, at 300 °C, and at 600 °C using a convection oven and a non-split tube furnace as shown in Fig. 6.

The second measured thermal property is the specific heat capacity. The equipment used was the differential scanning calorimetry DSC model 3+ from Mettler Toledo (Greifensee, Switzerland). The samples were homogenized through grinding to a powder size of less than 0.063 mm. A cement sample containing 7 ± 2 mg was filled into 40 ml aluminium crucibles. To determine the specific heat capacity, the target thermal cycle profile was first obtained using sapphire. The thermal cycle to which the CAC and RC specimens after 0 and 25 thermal cycles were subjected was set between 15 °C and 400 °C with a heating rate of 10 °C/min. The test was carried out in nitrogen condition at constant pressure and with a flow of 50 mL/min.

The compressive testing procedure involves the application of a load to samples side faces using a testing machine Matest (Treviolo, Italy) according to the UNI EN 1015–11:2019 [36]. During testing, a constant loading rate of 0.5 MPa/s is maintained until fracture occurs. Accordingly, the compressive strength is determined using the following formula:

$$R_c = \frac{F_c}{1600} \quad (5)$$

where R_c represents the compressive strength in N/mm^2, F_c is the maximum load applied to the specimen in N, and 1600 is the area of the platens or auxiliary plates (40 mm × 40 mm).

Finally, the XRD and petrographic analysis were performed. The crystalline phases of concretes before and after the thermal cycles were determined with the X-ray diffraction (XRD) test. The diffractometer Siemens EM-10110BU model D5000 (Munich, Germany) with CuKα radiation was used for this purpose. The samples were ground into a size 5 powder μm and the following parameters were considered in the test, position 5–70 2Θ, 0.05 step size and 3 s as scan step time. The interpretation of the data was carried out using PANalytical B.V. software. Instead, the petrographic analysis served to verify the mineralogical composition, the microstructure of the samples and the interface between cement paste and aggregate. The same petrographic analysis examined the porous structure within the matrix. To obtain the thin petrographic section, a 50 × 50 mm concrete specimen was stabilized using epoxy resin and once hardened a cross section, 30 μm thick and dimensions 50 × 30 mm, is sliced. A "Motic" model binocular lens and a camera model "Euromex" with 10 MP and a Nikon Eclipse E200 optical microscope, using the polarized light microscope method, were used to interpret the data.

4. Results

First the new formulation was developed. The process followed to obtain the fineness modulus of the aggregates was to sieve them according to the series of standardized sieves of ISO 3310–2:1999. Once the materials were sieved, the results were represented in a graph. On the ordinate axis, the percentages that accumulated through each sieve were placed on a decimal scale; on the abscissa, the opening of the sieves was placed on a decimal logarithmic scale.

In the same graph, the Fuller parabola was represented in green, which was taken as a reference for the optimal theoretical curve for the granulometric mixture of the various sizes of aggregates. Fuller parabola favours compactness, avoiding segregation through homogeneity, offering a good study of the granulometry of the aggregates, which results in good workability of the concrete in its fresh state [37]. Both the concrete and refractory industries, in their corresponding dosages, seek to obtain a structure that is as dense as possible by optimizing the packing of the material through a detailed study of the particles size to achieve a low viscosity mixture. Achieving 100 % packing density is impossible, but careful particle size distribution can control the rheology and govern the properties of unshaped refractory concretes.

Fig. 7 represents in a dotted line the granulometric curve continuous in sizes and adjusted to the Fuller parabola that was deduced from the mixing percentages of the aggregates used: chamotte and basalt. To consider that a curve is adjusted, it is not necessary that the proportions of the aggregates for each sieve coincide with all those corresponding to the theoretical reference curve. It is enough that the areas between the proposed curve and the reference one, located above and below it, coincide, which indicates that both curves have the same granulometric module.

A total of 25 cubic specimens of 100 × 100 × 100 mm were prepared with the dosage indicated in Table 4. The EN-14647: 2006 standard

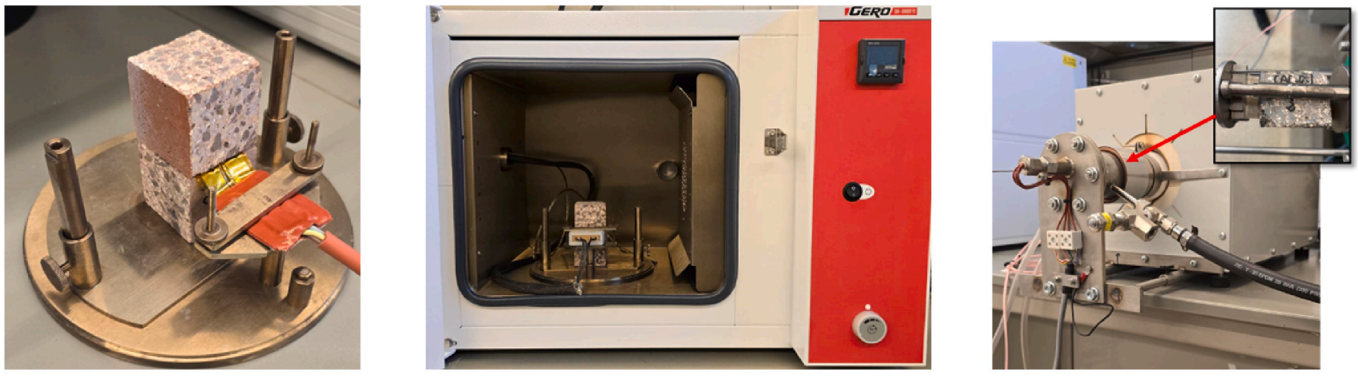

Fig. 6. Thermal conductivity measurement setup: (a) room temperature, (b) convection oven, and (c) non-split tube furnace.

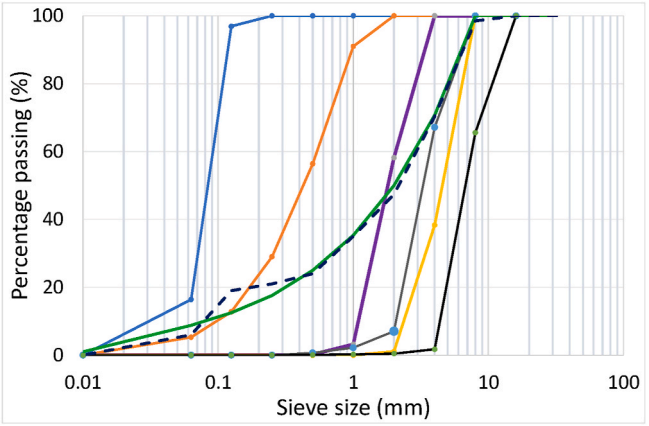

Fig. 7. Particle size distribution curve adjusted to the Fuller curve.

Table 4
Dosage of concrete selected (laboratory conditions: temperature = 21 °C, relative humidity = 49 %).

Materials	Percentage by volume of aggregates	Dosage (kg/m^3)
Chamotte filler (0–0.1 mm)	18 %	335.5
Chamotte filler (0–1 mm)	10 %	186.5
Chamotte sand (1–3 mm)	32 %	596.8
Chamotte gravel (2–5 mm)	12 %	223.8
Basalt gravel (3–5 mm)	8 %	165.8
Basalt coarse aggregate (6–10 mm)	20 %	414.4
CAC	–	425
Water	–	170
Super plasticizer (2 % of cement weight)	–	8.5
Total fresh concrete (kg/m^3)	–	2526.32
Water/cement ratio	0.4	
Slump	90 mm	

recommends a minimum CAC content of 400 kg/m^3 to achieve high initial compressive strengths and compensate for the intrinsic conversion phenomena of CAC [27]. In this study, 425 kg/m^3 were used because, when the working temperature is not very high, the ceramic bonds are partially achieved. In this case, the maximum working temperature is 700 °C, which for a monolithic refractory is a low temperature. By increasing the cement dosage, the mechanical strength at any temperature increases.

Different tests were necessary to achieve a fresh concrete of soft consistency (90 mm) in the Abrams slump test with sufficient workability to adopt the shape of the moulds. The results obtained were grouped into two variants: a very dry fresh concrete impossible to place; or a very fluid fresh concrete that could not be accepted either, since it favoured the segregation of its components, leaving the cement paste on top (Fig. 8).

Unshaped refractory concretes require certain proportions of water for their preparation. The amount of mixing water required increases with the lime content. A significant percentage of water reacts with the CAC forming hydrated products and the remainder is necessary for correct placement, although it is not part of the reactions, which generates porosity in the material after sintering. This reduces the characteristics of refractory concretes subjected to high temperatures. In the dosage used, the percentage by weight of water represents 6.8 % of the total, lower than 7 %, which is the maximum limit indicated for unshaped refractory concrete with low cement castable (LCC). LCC concretes require a water content of 3–7 % depending on their working temperature, although all of them are characterized by high density, low porosity, and high resistance to temperature and corrosion [38].

Fig. 8. Segregation of the components.

In the dosage presented in Table 4, 28 % of the total volume of aggregates consists of fractions less than 1 mm and 18 % less than 0.1 mm, very fine chamotte fractions that allow for close contact with the CAC fractions with sizes less than 0.063 mm. The purpose is to bring the finest fractions of CAC and chamotte as close as possible to allow, through contact, the creation of concave and convex surfaces, reaching a maximum green packing density, minimizing the amount of water used to fill the voids between particles. This step is important for the formation of the "ceramic bond" which, upon its first use, must transform an aluminous cement concrete into a refractory concrete based on aluminous cement and refractory aggregates.

However, for a defined amount of water, the fluidity of unshaped refractory concrete increases as the fraction of fine aggregates increases with respect to coarse aggregates. When the percentage of fine particles is important as in the case at hand, viscosity becomes a critical factor to consider. The finest fraction of the aggregates is responsible for the surface forces that occur at the solid – liquid interface and end up governing the dispersion and rheology of the particles in the fresh concrete.

The different dosage tests carried out in the laboratory resulted in a strong tendency for the smallest particles to agglomerate, forming weak groups. To counteract the formation of agglomerates, the amount of water can be increased, which harms the resistance of the refractory concrete due to the larger number of pores formed and segregation can occur when the amount of water is added in excess (Fig. 9). Another option is the use of dispersing agents that deagglomerate small particles, resulting in a mixture with good workability and low viscosity. These dispersing agents are known as superplasticizing additives. Relevant research has shown that polycarboxylate ethers (PCE) are more effective additives than polyacrylates (PA) in silica-alumina systems [39,40] Two polycarboxylate ethers were tested: Sika Viscocrete-20HE and Sika Viscocrete-90NG. The first is a high-performance superplasticizer suitable for structural self-compacting concretes whose results were not as expected. The second is a new generation, high-performance superplasticizer that increased the rheology of the mixture by adding 2 % of the weight of the cement, the maximum percentage recommended by the manufacturer.

The analysis of the produced samples started with the visual inspection of samples before cycling, that revealed few small surface voids both for CAC and RC but this characteristic did not influence on the damage of the samples. Indeed, after cycling there was not the formation of any superficial microcracks (Fig. 9). The only significant result is the change in colour after cycling of CAC sample (Fig. 9a) which is similar to that of RC sample (Fig. 9b). If before cycling grey and black tones are appreciated, after cycling the relevant tones are clearly earthy, typical of refractory ceramic materials.

Fig. 10 shows the apparent density values of CAC and RC samples before and after cycling. CAC has higher initial density than RC samples, 2419.83 kg/m^3 and 2335.89 kg/m^3, respectively, but after 25 cycles it presents a notable loss up to reaching the value of 2317.49 kg/m^3 while

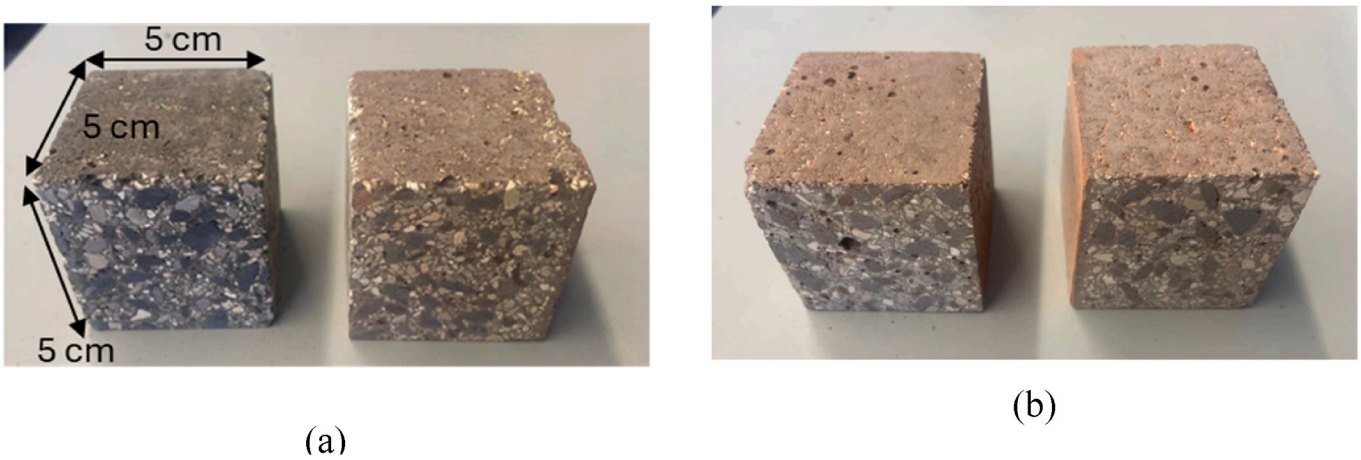

Fig. 9. Visual inspection before and after cycling of (a) CAC and (b) RC samples.

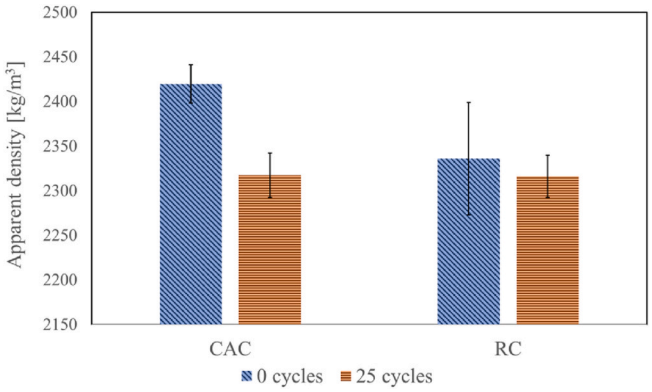

Fig. 10. Apparent density results.

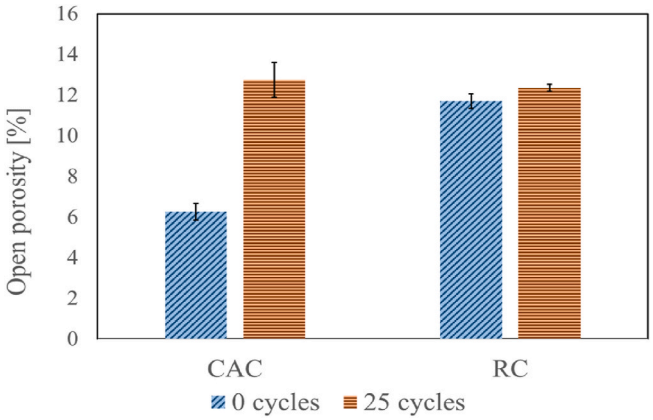

Fig. 11. Porosity test results before and after cycling.

the RC samples remain almost constant with a final value of 2316.41 kg/m^3. This result is confirmed by the weight loss which is approximately 5 % for CAC and 0.3 % for RC, as reported in Table 5.

The porosity values of the CAC and RC samples are shown in Fig. 11 and are in accordance with the density trend. Indeed, the porosity of CAC increases after 25 cycles, going from values around 6 % to values of almost 13 % with a notable loss of density. Instead, the RC values remain constant around 12 %.

Fig. 12 shows the thermal conductivity of the concrete samples (CAC and RC) measured at room temperature. The thermal conductivity of RC remains almost constant after 25 cycles, while that of CAC decreases from 1.66 W/m·K to 1.10 W/m·K after 25 cycles. This result is directly connected to the CAC samples increased porosity after cycling and, therefore, to the formation of a more voids and a reduction in the thermal conductivity.

Subsequently, the thermal conductivity of concrete samples (CAC and RC) was also measured at 300 °C and 600 °C to analyse the variation of samples thermal performance at high temperatures. All concrete samples, except the CAC 0 samples, showed an increasing trend in thermal conductivity with temperature (Fig. 13). At 25 °C, the pores of CAC 0 cycles contain moisture and this influences the thermal

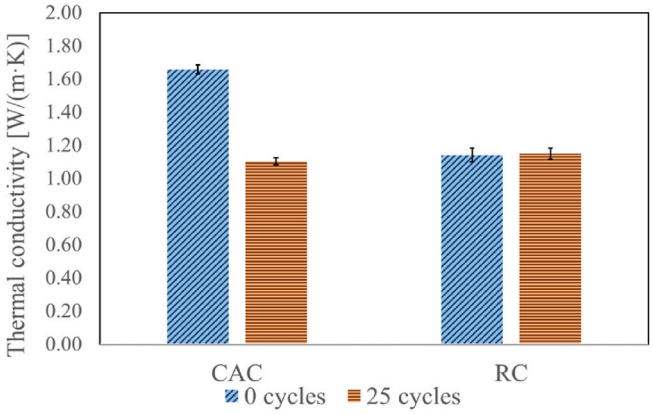

Fig. 12. Thermal conductivity plot of the concrete samples CAC and RC at room temperature before and after cycling.

Table 5
CAC and RC weight loss.

Sample	Weight loss (%)	
	Average	Standard deviation
CAC	4.99	0.89
RC	0.30	0.01

conductivity (1.60 W/m·K). At 300 °C, capillary water loss is complete and the gel water loss of calcium aluminate cement begins, which is complete at 400 °C. Water loss, whether capillary or combined, can justify the value of the reduction in thermal conductivity of CAC 0 cycles at 300 °C (1.30 W/m·K) [41]. At 600 °C, CAC 25 cycles, RC 0 cycles, and RC 25 cycles samples showed similar percentage increments (48 %, 48 %, and 50 %) compared to room temperature, respectively. These results are in agreement with those presented by Verdeja et al. [42], where the evolution with temperature of the thermal conductivity of

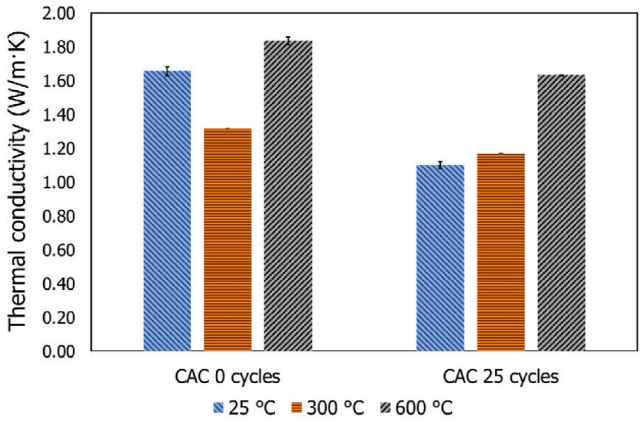

(a)

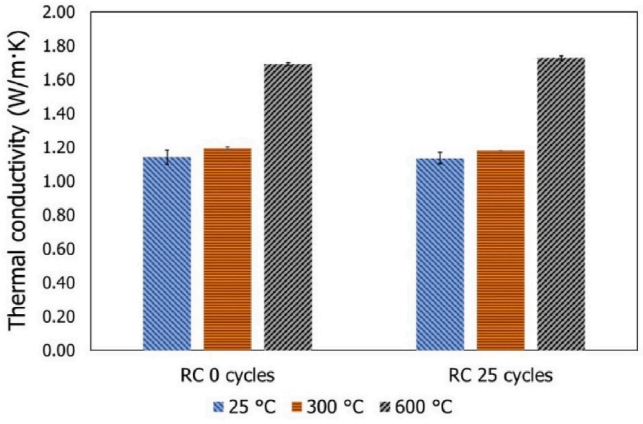

(b)

Fig. 13. Thermal conductivity vs temperature plot of the concrete samples (a) CAC and (b) RC measured before and after cycling.

silico-alumina refractory materials is shown from 200 °C to 1200 °C; at 600 °C a thermal conductivity of 1.65 W/m·K is assigned.

Further, the thermal conductivity measurements at room temperature were also performed on three distinct faces of the same pair of RC samples to verify the homogeneity of the compound. Table 6 shows the values obtained, proving that the developed samples are isotropic, with no significant variation in the thermal conductivity across different sides of the samples.

Fig. 14 reports the variations in the specific heat of CAC and RC samples obtained during consecutive heating (15 °C to 400 °C) and cooling (400 °C and 15 °C) cycles, respectively. The specific heat trend was identical across all samples and increased from ~0.9 to ~1.3 J/g·K with temperature during the heating cycle. A similar behaviour was observed during the cooling cycle, but vice versa; the specific heat values decreased from ~1.3 to ~0.9 J/g·K with temperature. The specific heat capacity increased after thermal cycling. More in detail, samples at 0 cycles show values from about 0.9 J/g·K to 1.3 J/g·K

Table 6
Variation of thermal conductivity measured on three distinct faces of the same pair of RC samples.

Thermal conductivity [W/m·K]				
Side 1	Side 2	Side 3	Average	Standard deviation
1.15	1.135	1.185	1.157	0.026

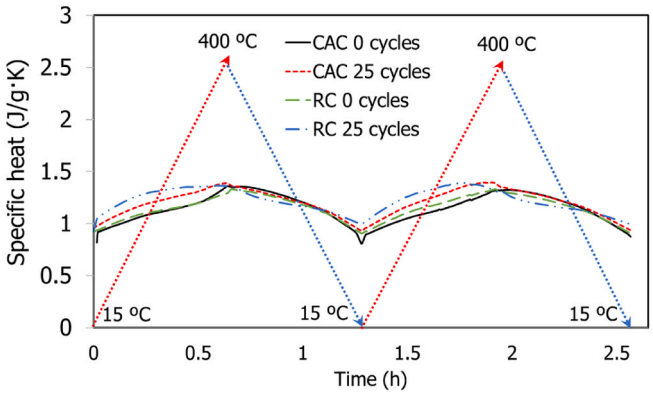

Fig. 14. Specific heat curves of concrete samples CAC and RC before and after cycling.

between 15 °C and 400 °C. In the same range of temperatures, samples at 25 cycles reached values from 1.0 J/g·K to 1.4 J/g·K.

Table 7 shows the specific heat values of the concrete samples averaged over the temperature range during the heating and cooling cycle. The values are found to be almost similar across the developed concrete formulations.

Mechanical performance is presented in Fig. 15. RC keeps the compressive strength almost unchanged after 25 cycles, despite the initial values being much lower than those of CAC (100.42 MPa versus 64.28 MPa). CAC samples reduce their compressive strength by almost 50 % as could be expected from the porosity and density results. The final compressive strength value after 25 cycles is 51.83 MPa, which is within the range of high-strength concretes (>50 MPa); this is not a residual strength.

The reduction in compressive strength is also confirmed by visual inspection of the tested samples before and after cycling (Fig. 16). RC samples only broke at the corners while the CAC samples show deeper damage.

The changes observed in refractory concretes at a macro level must have an explanation at a micro level. The crystalline phases of the concretes CAC_0 cycles, RC_0 cycles, and RC_25 cycles are presented in Fig. 17, through a mineralogical analysis by X-ray diffraction (XRD). The samples present a large number of crystalline phases with a notable overlap of the diffraction peaks that makes the interpretation of the diffractograms difficult.

The hydraulic phases of the CAC cement paste are responsible for reducing the porosity and increasing the mechanical resistance of the concrete until the solid-state sintering process begins at around 800 °C for this dosage. During the first thermal cycle, the dehydration of the compounds begins and subsequent cycling induces greater chemical transformations.

Through XRD analysis it can be seen that CAC_0 cycles present a large number of crystalline phases with a considerable overlap of diffraction peaks. The incorporation of very fine fractions of kaolin calcined at 1400 °C (chamotte) as aggregate in the dosage, allows the identification of mullite ($Al_{4.59}Si_{1.431}O_{9.7}$; PDF 79–1455) as the majority phase by 13 %, along with quartz low (SiO_2; PDF 65–0466) by 14.3 %, and cristobalite high (SiO_2; PDF 85–0621) by 8.2 %, and minor amounts of hematite (Fe_2O_3; PDF 87–1164) by 3 % and corundum (Al_2O_3; PDF 89–3072) by 1.6 %. Peaks of other common minor components of aluminous cement were also identified, such as gehlenite ($Ca_2Si_{1,25}Al_{1,75}O_7$; PDF 79–2422) by 2 % and brownmillerite ((Ca_2Al, $Fe{+}3)_2O_5$; PDF 30–0226) by 3 %. In turn, two hydrated crystalline phases are identified: hydrogarnet ($Al_2O_3.(CaO)_3.(H_2O)_6$, C_3AH_6; PDF 76–0557) by 3.4 % and gibbsite ($Al(OH)_3$, AH_3; PDF 76–1782) by 2.7 %, which offer hydraulic bonding and are responsible for increasing the mechanical resistance until the sintering process begins [43]. The presence of the stable hydrate C_3AH_6 shows that the concrete at room

Table 7
Specific heat values obtained for the concrete samples.

Temperature (°C)	Specific heat (J/g·K)							
	CAC 0 cycles		CAC 25 cycles		RC 0 cycles		RC 25 cycles	
	Heating	Cooling	Heating	Cooling	Heating	Cooling	Heating	Cooling
50	0.95	0.96	1.02	1.00	0.97	0.97	1.11	1.04
100	1.01	1.07	1.10	1.09	1.03	1.07	1.20	1.10
150	1.06	1.16	1.17	1.16	1.09	1.14	1.27	1.14
200	1.10	1.22	1.22	1.21	1.12	1.19	1.31	1.17
250	1.14	1.28	1.26	1.26	1.15	1.24	1.34	1.20
300	1.18	1.32	1.29	1.30	1.18	1.28	1.35	1.24
350	1.25	1.35	1.35	1.34	1.24	1.31	1.36	1.29
400	1.36	1.36	1.39	1.39	1.29	1.29	1.36	1.36
Average	1.13	1.21	1.23	1.22	1.13	1.19	1.29	1.19

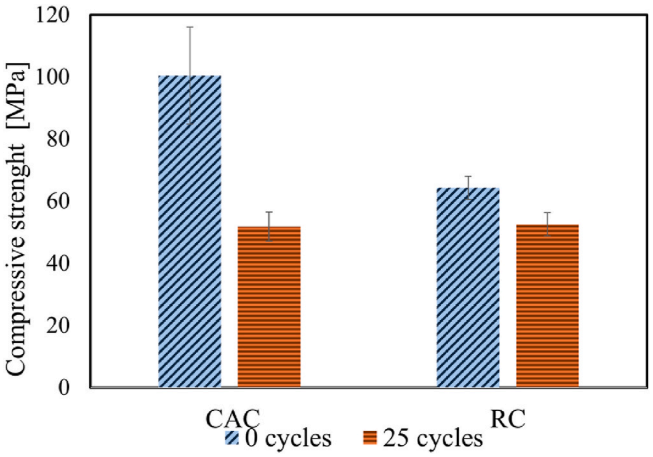

Fig. 15. Mechanical results before and after samples cycling.

temperature has already started the conversion reaction to transform into a stable cubic network, releasing a large amount of water through evaporation. Simultaneously, the stiffening of the gibbsite occurs, which crystallizes and contributes to the permeability of the structure [44]. From this moment, and as long as the conversion process does not progress, there are no significant changes in the physical properties of the concrete.

The XRD of the first thermal cycle that reaches 800 °C and initiates the main transformations of the crystalline phases is shown in Fig. 18b. The diffractogram does not detect the two aforementioned hydrated crystalline phases. On the other hand, it does detect mayenite ($Ca_{12}Al_{14}O_{33}$; PDF 78–0910) by 1.6 % and calcium monoaluminate ($CaAl_2O_4$, CA; PDF 70–0134) by 11.4 %, which are anhydrous phases. Probably the water content remaining in the material was reduced by evaporation and boiling. These main anhydrous phases are similar to those reported in white aluminous cement concretes with 50 % by weight of Al_2O_3 [45]. Likewise, the anhydrous crystalline phases obtained agree with those of other studies on the thermomechanical behaviour of CAC at temperatures above 450 °C [46] and even after 25 cycles up to 550 °C [47]. The diffractogram also detects gehlenite ($Ca_2Si_{1,25}Al_{1,75}O_7$, C_2AS; PDF 79–2422) by 1.6 %, a crystalline phase where SiO_2, CaO, and Al_2O_3 appear for the first time in combination, which are oxides always present in the composition of a silicoaluminous refractory concrete.

After 25 thermal cycles (Fig. 18c), the diffractogram does not detect the previously described mayenite, gehlenite or calcium monoaluminate, which are the result of the dehydration of the CAC cement and necessary for the formation of the ceramic bond. Only the finest part of the chamotte aggregates participates in the ceramic bond formation reaction depending on the temperature reached. The products that generally appear above 800 °C are anorthite ($CaO.Al_2O_3.2SiO_2$; CAS_2) and gehlenite ($2CaO.Al_2O_3.SiO_2$; C_2AS) [48]. However, the diffractogram detects the stable hydrate gibbsite ($Al(OH)_3$, AH_3; PDF 76–1782) by 2.1 %.

As the cycling and its corresponding thermal treatment are carried out, the formation of the mullite phase ($Al_{4,59}Si_{1,41}O_{9,7}$; PDF 79–1455) increases in percentage, i.e. it reaches 13 %, 18.2 %, and 24.7 %, for CAC_0 cycles, RC_0 cycles, RC_25 cycles, respectively. The mullite-type silicate phase is notable because, in these refractory concretes, it resists to high temperatures and thermal shock due to the strong reaction between alumina (Al_2O_3) and silica (SiO_2).

Four thin petrographic sections were made to check the

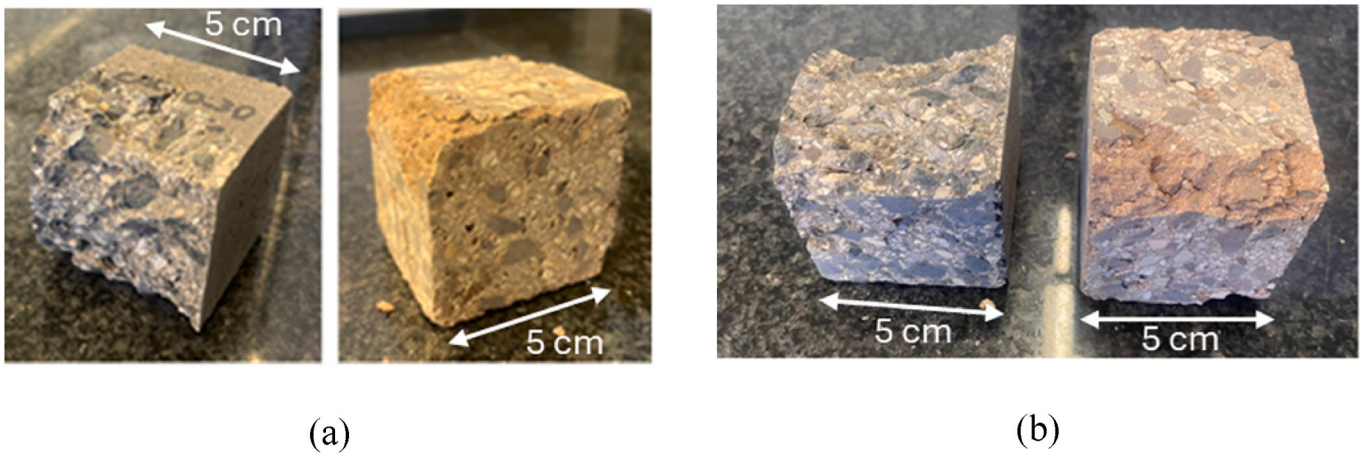

Fig. 16. Mechanical damage on CAC an RC samples (a) before and (b) after cycling.

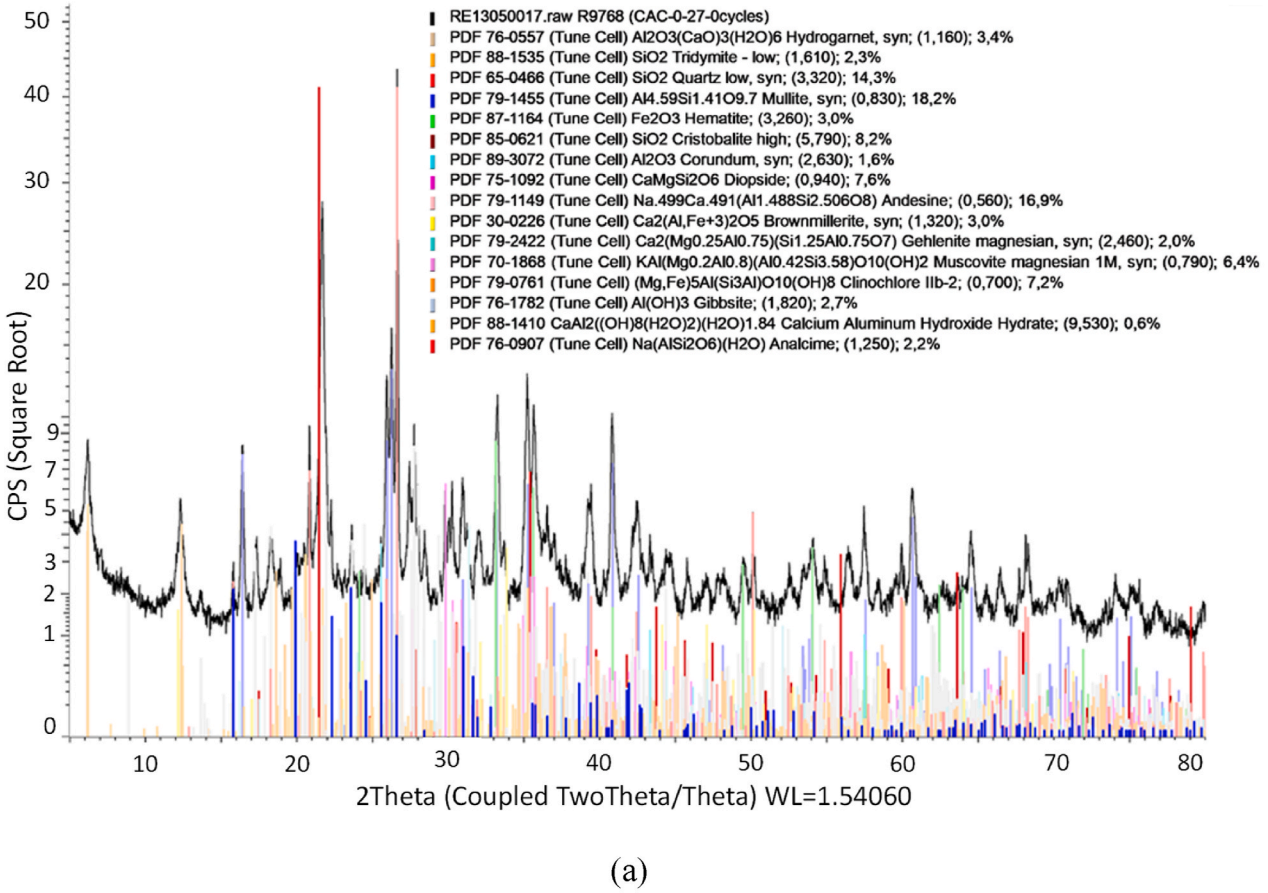

(a)

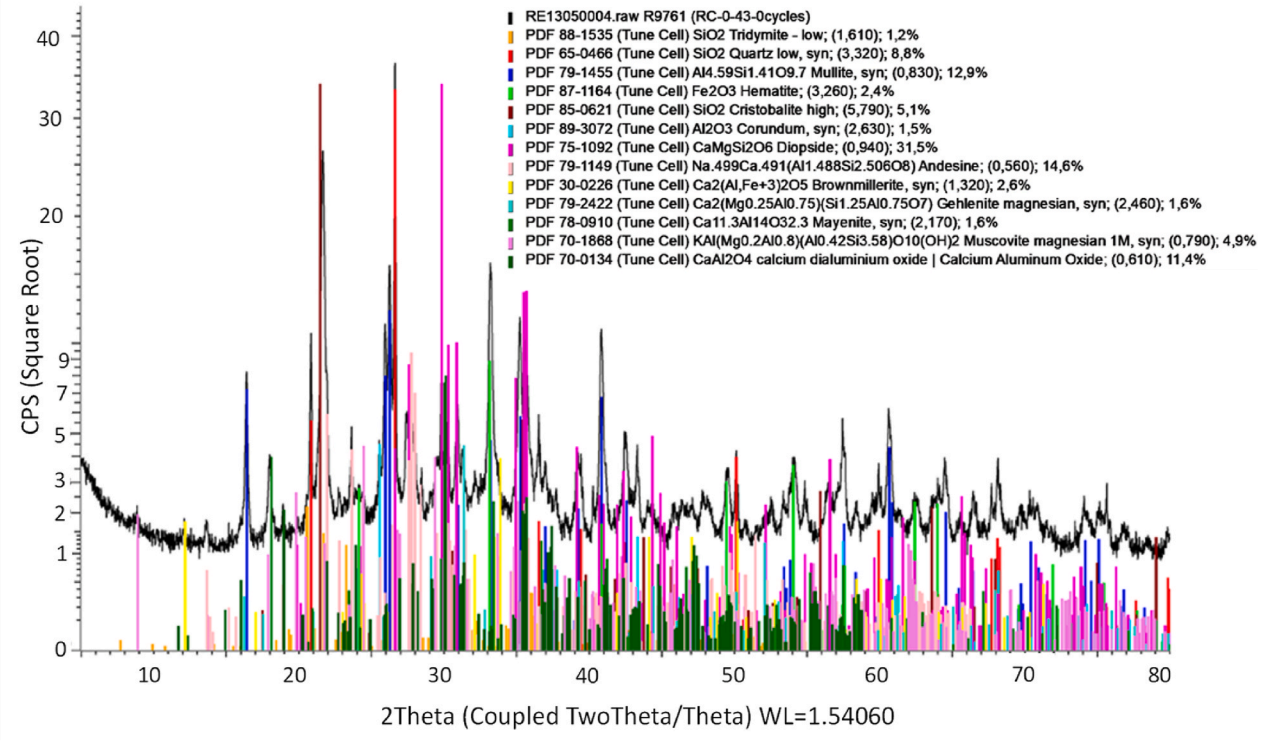

(b)

Fig. 17. XRD of a) CAC_0 cycles, b) RC_0 cycles, and c) RC_25 cycles.

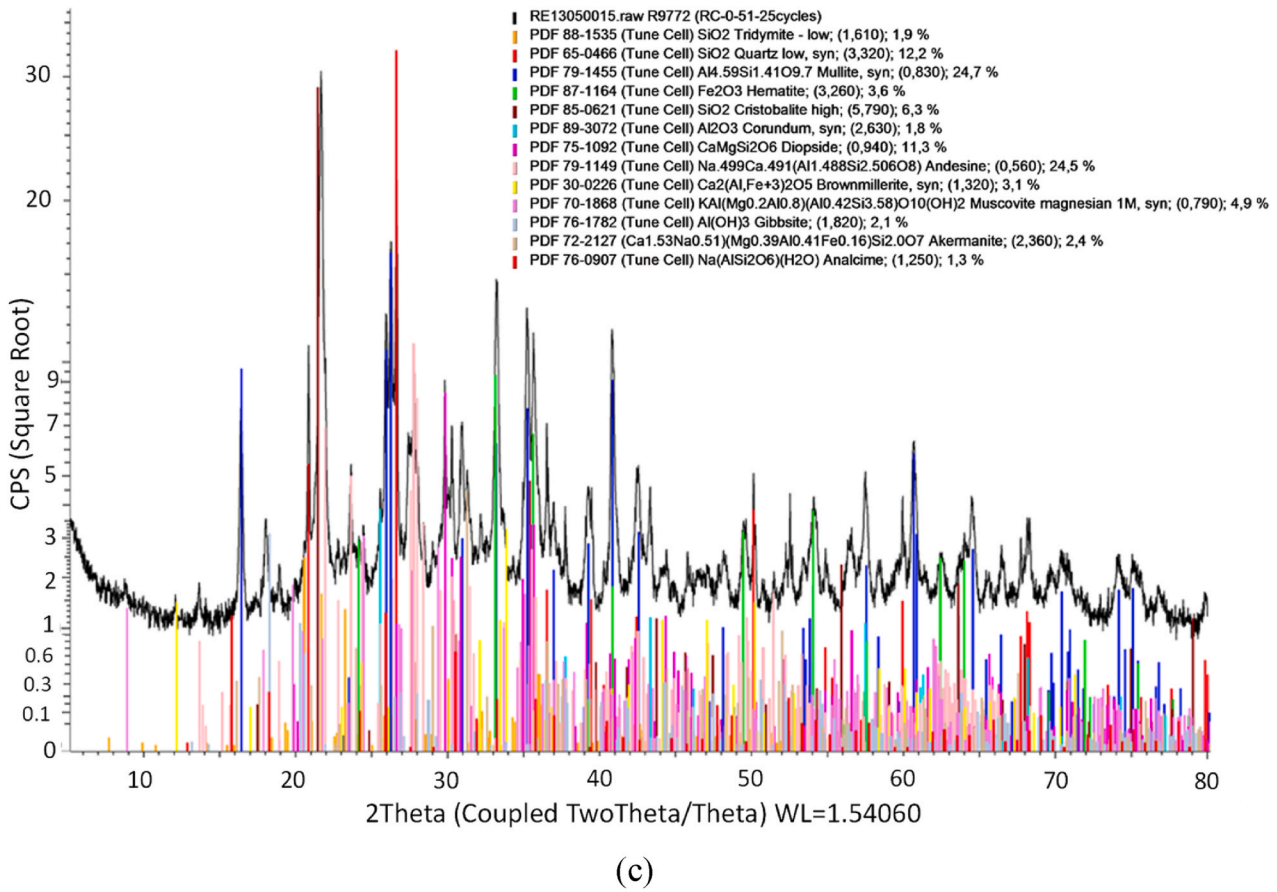

Fig. 17. (*continued*).

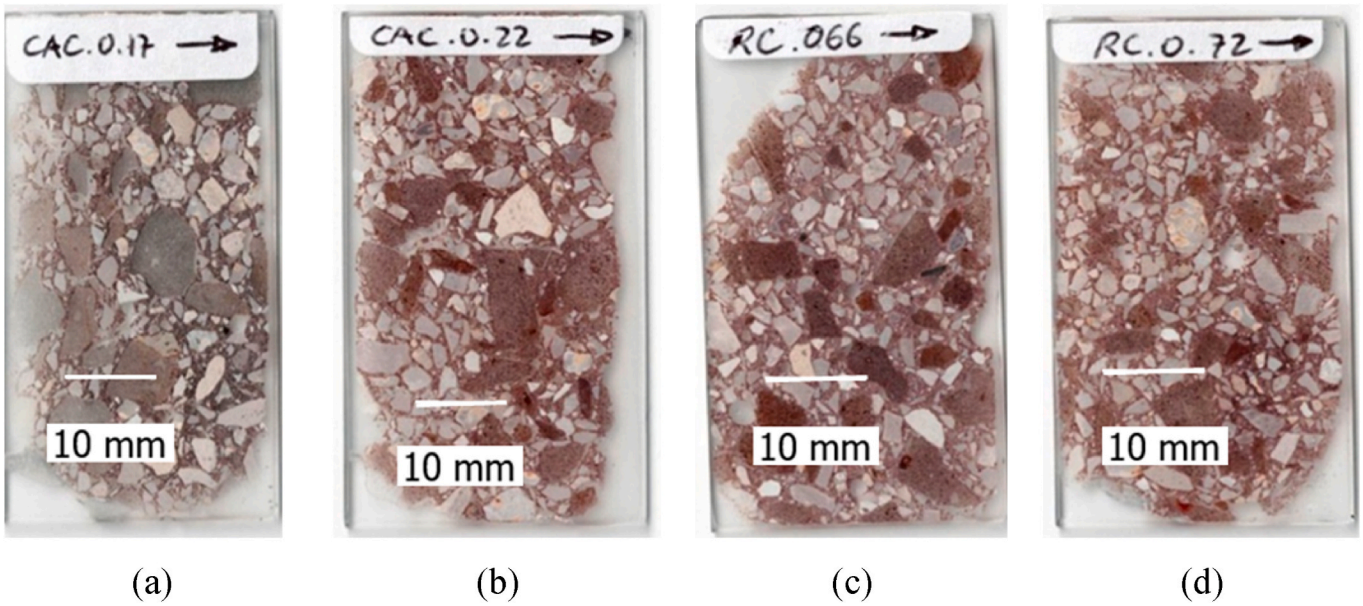

Fig. 18. Petrographic thin section of the concrete samples: (a) CAC before cycling, (b) CAC after cycling, (c) RC before cycling, and (d) RC after cycling.

mineralogical composition and the microstructure of the samples, identifying the interface between the cement paste and the aggregate, as well as to examine the porosity in the concrete matrix. The stabilized sheets are shown in Fig. 18.

At a macro level, no relevant colour changes of the materials are seen between the four sheets studied. In all of them, the intense black colour of the basalt aggregate and the range of white and grey colours of the chamotte aggregate can be observed, in similar proportions. The union of the various granulometries formed by the CAC cement paste does not seem to be significantly different after the thermal cycling of the samples.

Fig. 19 presents the petrographic analysis that determines the state of

the interface between the aggregates and the CAC cement paste before and after its thermal cycling in the samples CAC_0 cycles, RC_0 cycles, and RC_25 cycles. CAC_0 cycles is a concrete without heat treatment and whose bonds are hydraulic. RC_0 cycles is a concrete that underwent one thermal treatment cycle with the aim of developing ceramic bonds and transforming into a silico-aluminous refractory material. The RC_25 cycles underwent 25 thermal cycles.

The images stand out for the large amount of aggregate compared to the cement paste. The aggregates are angular and of low sphericity, according to the classification by Dapples et al. [49] and modified by Powers [50]. In this closer image, a change in colour of the basalt is observed, which changed from intense black to brown tones. In the image corresponding to RC_0 cycles captured with a binocular magnifying glass, it is observed that the union between the CAC and the chamotte aggregate is more cohesive than the union between the CAC and the basalt, since retraction cracks are observed in the union with the volcanic arid (indicated with blue arrow in RC_0 cycles). Apparently, a larger aggregate size leads to greater microcracking at the interface.

Other authors, such as John et al. [51], also highlighted this behaviour and suggested that it could be attributed to the difference in thermal expansion between the aggregates and the cement paste. In the same image, two small cavities were indicated with a green arrow that, despite the compaction vibration of the test tube, were not filled when the concrete was in a fresh state. A higher porosity is observed in the RC_25 cycles image compared to RC_0 cycles, with contact losses between aggregates that can reach values of 1 mm (indicated with a blue arrow in RC_25 cycles). These pores always form around the basalt and never around the chamotte. It should be noted that, after 25 cycles, no breakage cracks are observed that cut the aggregates and the degassing pores were not modified. In this case, it can be stated that the thermal properties of the different minerals that make up this concrete are similar and do not decompose at high temperatures.

Fig. 20 shows the petrographic analysis that determines the state of the interface between the aggregates and the cement paste CAC_25 cycles and RC_25 cycles.

The black spots that can be seen are pores that have formed after 25 thermal cycles. In both concretes, the pore density is very similar and they didn't increase in size or become interconnected. These images show that, most probably, the thermal treatment performed with the CAC_0 cycles sample to convert it into RC_0 cycles is not necessary, so this intermediate step can be avoided.

In stone materials, the predominant heat transfer mechanism is conduction. However, in high-porosity materials and at high temperature, radiation can significantly contribute to heat transfer in the pores. The thermal conductivity of stone materials is a function of their nature, microstructure, porosity, and working temperature [52]. In this sense, a high concrete density has a positive effect on the thermal storage process because it increases its thermal energy storage capacity. Thermal shocks during cycling can cause the formation of cracks and/or fissures along the interface and even permanent deformation in the analysed material. The level of cracking observed is related to the temperature reached, the number of cycles carried out, the anisotropic expansion of the minerals, and the low adhesion between the CAC paste and the basalt aggregate, especially the larger sizes between 6 and 10 mm incorporated in the concrete dosing.

A closer inspection of the concrete samples CAC_25 cycles and RC_25 cycles are presented in Fig. 21, where the microstructure of the materials is observed in greater detail. Two types of optical polarization microscope images were used, with the aim of showing the achievements more clearly. The white colour shows the pores and fractures in the petrographic sheet, while the rest of colours are related to the different minerals of the compound.

It is significant that, in both CAC_25 cycles and RC_25 cycles, spherical pores were detected, which help prevent the propagation of internal cracks by relaxing stresses. Regarding the type of cracks formed after 25 thermal cycles, these are concentrated at the interface around the basalt aggregate (6–10 mm), evidencing a weak bond in the CAC paste as a result of the released water and its consequent structural contraction.

However, this limited refractoriness is not observed in the other parts of the sample, where the CAC paste remains attached to the chamotte aggregate and the basalt aggregate (3–6 mm). This might be because the granulometry of the aggregates allows an optimal contact between particles and, in addition, thermal cycling could have consolidated the solid-state sintering mechanism of the silico-aluminous refractory material.

5. Discussion

Table 8 reports the comparison among the most significant test results of CAC and RC samples. The relative variation (Δ%) in any of the sample properties (x) was calculated following Eq. (6):

$$\Delta\% = \frac{x_i - x_f}{x_f}\ 100 \tag{6}$$

The evaluation of the variation before and after the thermal cycles (Δc%) was conducted considering x_i as the 0 cycles value and x_f the 25 cycles value. The variation between CAC and RC samples (Δs%) was calculated attributing the value of CAC sample to x_i and of RC samples to x_f.

CAC has higher initial density values but after 25 cycles the porosity increases reaching the same RC values which instead remain constant after cycling. This also affects the thermal conductivity and compressive strength of CAC which are reduced by 33 % and 48 % respectively. Both

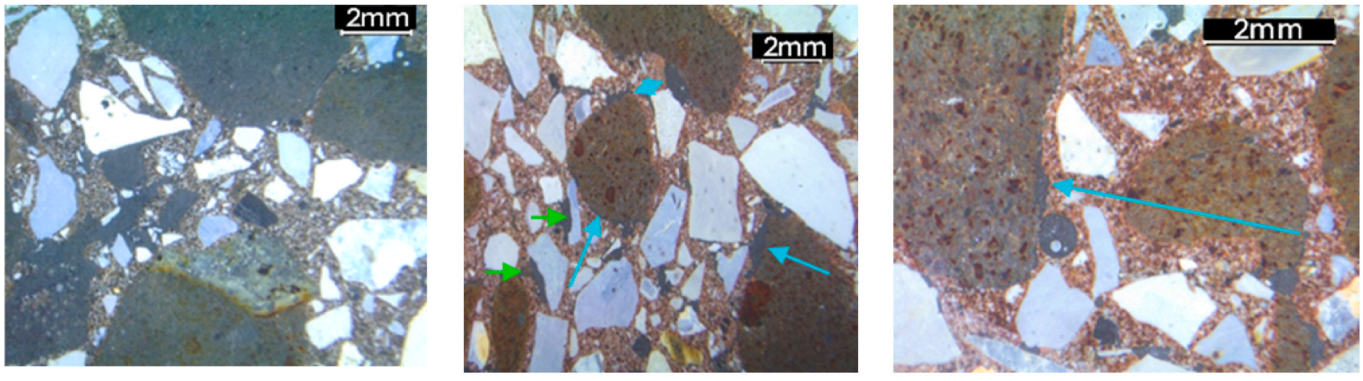

Fig. 19. Binocular loupe images of the concrete samples: (a) CAC before cycling, (b) RC before cycling, and (c) RC after cycling.

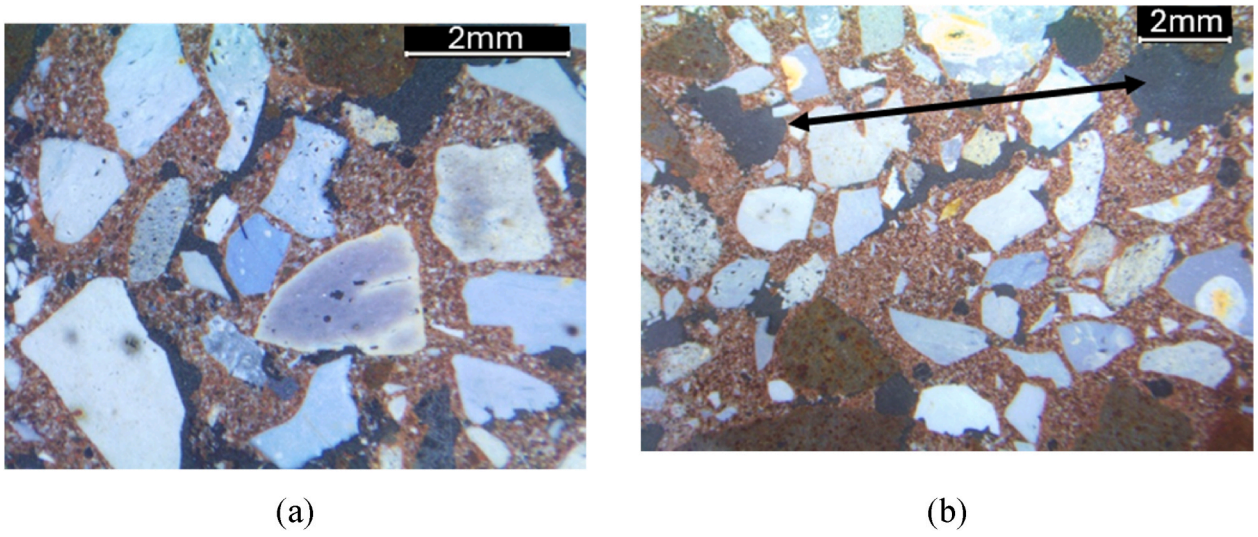

Fig. 20. Images of the concrete samples: (a) CAC after cycling and (b) RC after cycling.

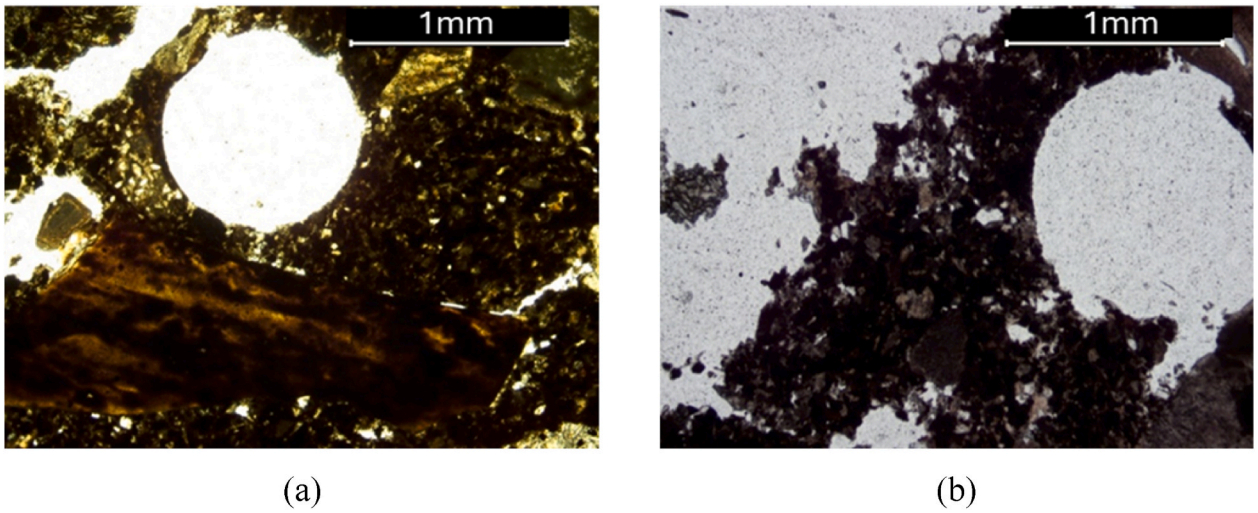

Fig. 21. Detailed images of the concrete samples: (a) CAC after cycling and (b) RC after cycling.

values after 25 cycles are however good especially if compared to that of the previous study [24] in which the compressive strength values only drop to less than 30 MPa after 10 treatment cycles due to the higher initial porosity (11 % versus just over 6 %). CAC sample after 25 cycles which worsens the thermal and mechanical performances, initially better than the RC. On the contrary, RC sample appears to be more stable as highlighted by the Δs% values assumed after the cycling for thermal conductivity and compressive strength. These results demonstrate that the new mix design is better suited to withstand high temperature applications. Concrete developed to be used as TES material, such as this one, should have enough mechanical performance to ensure that the TES tank will have the required self-preservation. One should remember that an ideal TES tank will not have any encapsulation that might give the TES component the required mechanical stability.

The increase in temperature inside the refractory concrete leads to changes in its physical properties that modify the mechanical properties of the material. The most relevant physical properties are thermal expansion, which depends mainly on the type of aggregate used; the porosity that occurs in the cement paste with increasing temperature; the density that is reduced basically by the loss of weight due to dehydration; and, the permeability that with increasing temperature is related to the level of degradation of the refractory concrete and the formation of microcracking [53]. These alterations lead to important changes in the mechanical properties of refractory concrete, affecting its compressive strength, tensile strength and yield strength. The increase in temperature causes a weakening of the paste-aggregate bond, leading to an increase in microcracking with the consequent loss of compressive strength. Tensile strength provides an order of magnitude of the capacity of a refractory concrete to resist cracking and is a parameter with greater sensitivity than compressive strength to the effects of temperature. Establishing analytical relationships between compressive strength and tensile strength of refractory concrete at high temperatures is not easy [54]. However, an analytical relationship between tensile and compressive strength for concretes with characteristic compressive strength ≤ C50/60 MPa can be found in the standard EN 1992-1-1:2013 [55]:

$$f_{ctm} = 0.30 f_{ck}^{2/3} \approx 10\% f_{ck}$$

where f_{ctm} is the average tensile strength of concrete and f_{ck} is the characteristic compressive strength of concrete.

That is, the average tensile strength of concrete is approximately 10 % of the compressive strength of concrete. The higher the compressive strength, the higher the tensile strength. The increase in temperature

Table 8
Comparison of the main CAC and RC samples results.

Sample	0 cycles	25 cycles	Δc%
Apparent density (kg/m^3)			
CAC	2419.83	2317.49	4.2
RC	2335.89	2316.41	0.8
Δs%	3.47	0.05	–
Open porosity (%)			
CAC	6.26	12.74	−103.6
RC	11.70	12.36	−5.6
Δs%	−86.90	3.02	–
Thermal conductivity – Room temperature (W/m·K)			
CAC	1.66	1.10	33.5
RC	1.14	1.15	−0.6
Δs%	31.15	−4.11	–
Thermal conductivity – High temperature (W/m·K)			
CAC	1.84	1.63	11.4
RC	1.69	1.73	−2.4
Δs%	8.15	−6.13	–
Compressive strength (MPa)			
CAC	100.42	51.83	48.4
RC	64.28	52.55	18.3
Δs%	35.99	−1.39	–

Where Δc% is the variation before and after the thermal cycles, and Δs% is the variation between CAC and RC samples.

inside the refractory concrete causes thermal expansion which translates into internal tensile stresses in the material causing microcracking, fissuring and possible decomposition. In refractory concrete, the predominant heat transport mechanism is conduction. Any microcrack or discontinuity in the material represents a loss of conduction, since the radiation that could occur in the cracks and/or pores is irrelevant.

The key results indicate that the initial heat treatment successfully achieved the ceramization of the new concrete formulation. Additionally, the thermal cycles performed are able to replicate the effects of the initial heat treatment. This suggests that in a real TES tank, the initial heat treatment may not be necessary, provided users can ensure that the temperature range and the heating and cooling rates of the thermal cycles closely match those of the initial treatment.

Moreover, the thermo-physical and mechanical properties of the new refractory concrete remain largely unaffected by the thermal cycles. Both its thermal conductivity and compressive strength demonstrate highly promising values for high-temperature TES applications.

The use of the concrete proposed in this study in bulk form is beneficial for the practical application because it is able to prevent several issues identified in a previous study related to the use of concrete for high temperature TES [7]. Specifically, the concrete can be used in a new modular design proposed in Ref. [7], which means that it doesn't require to be produced on-site (avoiding a few problems with on-site production, as described in Ref. [7]), it doesn't require the use of pipes for the heat transfer fluid (thus avoiding the issue of different thermal expansion coefficient of steel and concrete), it allows to use air as heat transfer fluid (thus avoiding the issue of compatibility between the heat transfer fluid - thermal oil or molten salts – and concrete, which moreover have limited operating temperature range), and solves the issue of oil/salt migration because of the direct contact with the concrete. The only issue that is not fully solved by the new concrete is its relatively low thermal conductivity, but this issue will be addressed in a future study. In addition, if the thermal conductivity of the concrete formulation can be enhanced, the modular design would also avoid the poor heat transfer problem associated with the gaps that might exists between the concrete modules that are stacked with each other. For the real application, the size and shape of the module and air channel should be optimised to achieve a good overall heat transfer of the concrete TES tank, which is out of the scope of this study, but will be addressed in a future publication.

6. Conclusions

In this study, a new concrete mix design containing refractory aggregates was produced and analysed in terms of thermo-physical, mechanical, and microstructural properties before and after 25 thermal cycles to simulate real application conditions at high temperatures. A comparison was performed between non-heat-treated (CAC) and heat-treated (RC) samples, but also between the CAC new mix design and the previous ones with silico-calcareous and steel-slag aggregates. Results demonstrated a better resistance to damage of the RC samples, which maintain their thermo-mechanical performance and porosity almost unchanged. The CAC samples worsen their initial behaviour but, after 25 thermal cycles, they reach values comparable with the RC samples and higher than the samples used in previous studies. Therefore, this new concrete formulation proved to have a very high potential to be used as TES material at high temperatures.

The main limitation of this study is the relatively low number of thermal cycles performed with the samples. Therefore, performing additional thermal cycles with the refractory concrete samples could be the objective of future studies. Further investigation will also focus on different ways to enhance even more the thermal conductivity and/or compressive strength, by using different components with additives with high thermal conductivity. Moreover, compatibility of the new refractory concrete with heat transfer fluids used in CSP plants will also be investigated.

CRediT authorship contribution statement

J. Ramon Castro: Writing – review & editing, Methodology, Investigation, Formal analysis, Data curation, Conceptualization. **Carolina Santini:** Writing – original draft, Visualization, Investigation. **Gabriel Zsembinszki:** Writing – review & editing, Formal analysis, Conceptualization. **Saranprabhu Mani Kala:** Writing – review & editing, Visualization, Investigation, Formal analysis, Data curation. **Franklin R. Martinez:** Writing – review & editing, Investigation. **Sara Risco:** Writing – review & editing, Investigation. **Claudia Fabiani:** Writing – review & editing, Supervision, Formal analysis. **Anna Laura Pisello:** Writing – review & editing, Supervision, Resources, Funding acquisition, Formal analysis. **Luisa F. Cabeza:** Writing – original draft, Supervision, Resources, Project administration, Methodology, Investigation, Funding acquisition, Formal analysis, Data curation, Conceptualization.

Declaration of competing interest

The authors declare that they have no known competing financial interests or personal relationships that could have appeared to influence the work reported in this paper.

Acknowledgements

This project has received funding from the European Union's Horizon 2020 Research and Innovation Programme under Grant Agreement 101036910 (StoRIES). This work was partially funded by the Ministerio de Ciencia e Innovación - Agencia Estatal de Investigación (AEI) (PID2021-123511OB-C31- MCIN/AEI/10.13039/501100011033/ FEDER, UE and RED2022-134219-T). This study received funding from the Ministerio de Ciencia e Innovación - Agencia Estatal de Investigación (MCIN/AEI/10.13039/501100011033) through the PCI2020-120695-2 project and the European Union "NextGenerationEU"/PRTR". The authors from University of Lleida would like to thank the Catalan Government for the quality accreditation given to their research group (2021 SGR 01615). GREiA is certified agent TECNIO in the category of technology developers from the Government of Catalonia. This work is partially supported by ICREA under the ICREA Academia programme. This work was partially funded by the European Union—NextGenerationEU under Italian Ministry of University and Research

(MUR) National Innovation Ecosystem grants ECS00000041— VITALITY—CUP J97G22000170005 and CUP B43C22000470005. The authors thank the PhD school in Energy and Sustainable Development at CIRIAF University of Perugia.

Data availability

Data will be made available on request.

References

[1] M. Simona, G. Badea, A. Enache, C. Filote, R. Gabriel, M. Rata, A. Lavric, R. Felseghi, Concentrating Solar Power Technologies, 2019, pp. 1–17, https://doi.org/10.3390/en19061048.
[2] U. Pelay, L. Luo, Y. Fan, D. Stitou, M. Rood, Thermal energy storage systems for concentrated solar power plants, Renew. Sustain. Energy Rev. 79 (2017) 82–100, https://doi.org/10.1016/j.rser.2017.03.139.
[3] R. Kunwer, S. Pandey, G. Pandey, Technical challenges and their solutions for integration of sensible thermal energy storage with concentrated solar power applications — a review, Process Integration and Optimization for Sustainability (2022) 559–585, https://doi.org/10.1007/s41660-022-00231-9.
[4] O. Achkari, A. El Fadar, Latest developments on TES and CSP technologies – energy and environmental issues , applications and research trends, Appl. Therm. Eng. 167 (2020) 114806, https://doi.org/10.1016/j.applthermaleng.2019.114806.
[5] G. Mohan, M.B. Venkataraman, J. Coventry, Sensible energy storage options for concentrating solar power plants operating above 600 °C, Renew. Sustain. Energy Rev. 107 (2019) 319–337, https://doi.org/10.1016/j.rser.2019.01.062.
[6] L. Boquera, J.R. Castro, A. Laura, L.F. Cabeza, Research progress and trends on the use of concrete as thermal energy storage material through bibliometric analysis, J. Energy Storage 38 (2021) 102562, https://doi.org/10.1016/j.est.2021.102562.
[7] L.F. Cabeza, D. Vérez, G. Zsembinszki, E. Borri, C. Prieto, Key challenges for high temperature thermal energy storage in concrete—first steps towards a novel storage design, Energies 15 (2022), https://doi.org/10.3390/en15134544.
[8] S. Khare, M.D. Amico, C. Knight, S. Mcgarry, Solar Energy Materials & Solar Cells Selection of materials for high temperature sensible energy storage, Sol. Energy Mater. Sol. Cell. 115 (2013) 114–122, https://doi.org/10.1016/j.solmat.2013.03.009.
[9] S. Wang, A. Abdulridha, J. Bravo, C. Naito, S. Quiel, M. Suleiman, C. Romero, S. Neti, A. Oztekin, Cement and Concrete Research Thermal energy storage in concrete : review , testing , and simulation of thermal properties at relevant ranges of elevated temperature, Cem Concr Res 166 (2023) 107096, https://doi.org/10.1016/j.cemconres.2023.107096.
[10] T. Lucio-martin, M. Roig-flores, M. Izquierdo, M.C. Alonso, Thermal conductivity of concrete at high temperatures for thermal energy storage applications : experimental analysis, Sol. Energy 214 (2021) 430–442, https://doi.org/10.1016/j.solener.2020.12.005.
[11] E. Tolentino, F.S. Lameiras, A.M. Gomes, C.A. Rigo Da Silva, W.L. Vasconcelos, Effects of high temperature on the residual performance of Portland cement concretes, Mater. Res. 5 (2002) 301–307, https://doi.org/10.1590/S1516-14392002000300014.
[12] Q. Ma, R. Guo, Z. Zhao, Z. Lin, K. He, Mechanical properties of concrete at high temperature — a review, Constr. Build. Mater. 93 (2015) 371–383, https://doi.org/10.1016/j.conbuildmat.2015.05.131.
[13] J. Xiao, Q. Xie, W. Xie, Study on high-performance concrete at high temperatures in China (2004 – 2016) - an updated overview, Fire Saf. J. 95 (2018) 11–24, https://doi.org/10.1016/j.firesaf.2017.10.007.
[14] C. Shi, Z. Wu, J. Xiao, D. Wang, Z. Huang, Z. Fang, A review on ultra high performance concrete : Part I . Raw materials and mixture design, Constr. Build. Mater. 101 (2015) 741–751, https://doi.org/10.1016/j.conbuildmat.2015.10.088.
[15] L.T. Phan, High-strength concrete at high temperature – an overview, in: Utilization of High Strength/High Performance Concrete, International Symposium | 6th | | Freunde Der Bavingenieur, Leipzig, GE, 2002. https://tsapps.nist.gov/publication/get_pdf.cfm?pub_id=860408. (Accessed 1 November 2024).
[16] M. Khan, J. Lao, M.R. Ahmad, M. Kai, J. Dai, The role of calcium aluminate cement in developing an efficient ultra-high performance concrete resistant to explosive spalling under high temperatures, Constr. Build. Mater. 384 (2023) 131469, https://doi.org/10.1016/j.conbuildmat.2023.131469.
[17] M.C. Alonso, J. Vera-agullo, L. Guerreiro, V. Flor-laguna, M. Sanchez, M. Collares-pereira, Cement and Concrete Research Calcium aluminate based cement for concrete to be used as thermal energy storage in solar thermal electricity plants, Cem Concr Res 82 (2016) 74–86, https://doi.org/10.1016/j.cemconres.2015.12.013.
[18] L. Boquera, J.R. Castro, A.G. Fernandez, A. Navarro, A. Laura, L.F. Cabeza, Thermo-mechanical stability of concrete containing steel slag as aggregate after high temperature thermal cycles, Sol. Energy 239 (2022) 59–73, https://doi.org/10.1016/j.solener.2022.04.062.
[19] A. Lau, M. Anson, Effect of high temperatures on high performance steel fibre reinforced concrete, Cem Concr Res 36 (2006) 1698–1707, https://doi.org/10.1016/j.cemconres.2006.03.024.
[20] A. Baradaran-nasiri, M. Nematzadeh, The effect of elevated temperatures on the mechanical properties of concrete with fine recycled refractory brick aggregate and aluminate cement, Constr. Build. Mater. 147 (2017) 865–875, https://doi.org/10.1016/j.conbuildmat.2017.04.138.
[21] W.G. Fahrenholtz, G.E. Hilmas, Ultra-high temperature ceramics: materials for extreme environments, Scr. Mater. 129 (2017) 94–99, https://doi.org/10.1016/j.scriptamat.2016.10.018.
[22] L. Scheinherrová, M. Dolez, M. Keppert, E. Vejmelková, D. Kon, C. Robert, Virtual Special Issue Durability of Innovative Construction Materials and Structures High Temperature Durability of Fiber Reinforced High Alumina Cement Composites, vol. 162, 2018, pp. 881–891, https://doi.org/10.1016/j.conbuildmat.2018.01.076.
[23] L. Boquera, J.R. Castro, A. Laura, C. Fabiani, A.D. Alessandro, F. Ubertini, L. F. Cabeza, Thermo-mechanical stability of supplementary cementitious materials in cement paste to be incorporated in concrete as thermal energy storage material at high temperatures, J. Energy Storage 54 (2022) 105370, https://doi.org/10.1016/j.est.2022.105370.
[24] L. Boquera, J.R. Castro, A. Laura, C. Fabiani, A.D. Alessandro, F. Ubertini, L. F. Cabeza, Effect of the curing process on the thermomechanical properties of calcium aluminate cement paste under thermal cycling at high temperatures for thermal energy storage applications, J. Energy Storage 56 (2022) 106039, https://doi.org/10.1016/j.est.2022.106039.
[25] L. Boquera, J.R. Castro, A. Laura, C. Fabiani, A.D. Alessandro, F. Ubertini, L. F. Cabeza, Solar Energy Materials and Solar Cells Thermal and mechanical performance of cement paste under high temperature thermal cycles, Sol. Energy Mater. Sol. Cell. 231 (2021) 111333, https://doi.org/10.1016/j.solmat.2021.111333.
[26] S. Chinchón, C. Andrade, El cemento de aluminato de calcio, in: Aluminosi. Jornades de Debat, Unitat de Rehabilitació i Medi Ambient del CAATEEB, Barcelona, 2020, pp. 82–91.
[27] L. Boquera, J.R. Castro, A.L. Pisello, C. Fabiani, A. D'Alessandro, F. Ubertini, L. F. Cabeza, Effect of the curing process on the thermomechanical properties of calcium aluminate cement paste under thermal cycling at high temperatures for thermal energy storage applications, J. Energy Storage 56 (2022), https://doi.org/10.1016/j.est.2022.106039.
[28] J. Puig Montraveta, Hormigones especiales. Hormigones refractarios. Tomo II, Universitat Politècnica de Catalunya. Escuela Tecnica Superior de Ingenieros de Caminos, Canales y Puertos, 1994.
[29] Cements Molins, Aluminate (2024). https://www.Molins.Es/Cements/Products/Cemento-Aluminato-de-Calcio/Aluminite/.
[30] Chamota Arciresa. http://www.Arciresa.Es/Chamota.Html, 2024.
[31] Pedrera Cansaboia, Basalto. http://www.Pedreracansaboia.Com/Agricultura/El-Basalto/, 2024.
[32] M. Jiang, W. Chen, Y. Liu, Y. Du, T. Deng, Analysis and prospect of thermodynamic behavior of aluminosilicate solid waste during ceramization, Int. J. Appl. Ceram. Technol. (2024) 1317–1332, https://doi.org/10.1111/ijac.14705.
[33] EN 1936:2010, Natural Stone Test Methods - Determination of Real Density and Apparent Density, and of Total and Open Porosity, British Standards vol. 3 (2010).
[34] I. Asadi, P. Shafigh, Z.F. Bin Abu Hassan, N.B. Mahyuddin, Thermal conductivity of concrete – a review, J. Build. Eng. 20 (2018) 81–93, https://doi.org/10.1016/j.jobe.2018.07.002.
[35] ISO 22007-2:2022, Plastics- Determination of Thermal Conductivity and Thermal Diffusivity- Part 2: Transient Plane Heat Source (Hot Disc) Method, International Organization for Standardization, Geneva, Switzerland, 2022.
[36] EN 1015-11:2019, Methods of Test for Mortar for Masonry, BSI Standards Publication, 2019.
[37] V. Calderón Carpintero, Á. Rodríguez Saiz, C. Pérez Val, A. Martín de la Fuente, Manual de problemas de dosificación de hormigones (I), Universidad de Burgos, 2012.
[38] I.M.I. Bayoumi, E.M.M. Ewais, A.A.M. El-Amir, Rheology of refractory concrete: an article review, Bol. Soc. Espanola Ceram. Vidr. 61 (2022) 453–469, https://doi.org/10.1016/j.bsecv.2021.03.003.
[39] S. Otroj, A. Sagaeian, A. Daghighi, Z.A. Nemati, The effect of nano-size additives on the electrical conductivity of matrix suspension and properties of self-flowing low-cement high alumina refractory castables, Ceram. Int. 36 (2010) 1411–1416, https://doi.org/10.1016/j.ceramint.2010.02.008.
[40] C. Parr, B. Wöhrmeyer, B. Valdelievre, A. Namba, Effect of formulation parameters upon the strength development of calcium aluminate, in: TARJ Refractory Conference, Osaka, Japan, 2002, pp. 1–12.
[41] E. García Alcocel, E. Zornoza, O. Galao, P. Garcés, Durabilidad del cemento de aluminato de calcio (CAC), in: Procesos de Degradación Físico-Químicos En Estructuras de Hormigón Armado, Univeritat D'Alacant, 2021, pp. 201–233.
[42] L.F. Verdeja, J.P. Sancho, A. Ballester, Materiales Refractarios Y Cerámicos, Editorial Sintesis, 2008.
[43] W. Gu, L. Zhu, X. Shang, D. Ding, L. Liu, L. Chen, G. Ye, Effect of particle size of calcium aluminate cement on volumetric stability and thermal shock resistance of CAC-bonded castables, J. Alloys Compd. 772 (2019) 637–641, https://doi.org/10.1016/j.jallcom.2018.09.128.
[44] F. Faccin, A. F.P, A.G. Tomba Martinez, L. Ramajo, Evaluación de la resistencia al choque término de hormigones refractarios silicoaluminosos. Efecto del tratamiento térmico, Bol. Soc. Espanola Ceram. Vidr. 58 (2019) 246–254, https://doi.org/10.1016/J.BSECV.2019.05.002.
[45] W.G. Bareiro, F. de Andrade Silva, E.D. Sotelino, O. da F.M. Gomes, The influence of alumina content on the chemical and mechanical behavior of refractory concretes fired at different temperatures, Constr. Build. Mater. 187 (2018) 1214–1223, https://doi.org/10.1016/J.CONBUILDMAT.2018.08.065.
[46] V. Antonovič, J. Keriene, R. Boris, M. Aleknevičius, The effect of temperature on the formation of the hydrated calcium aluminate cement structure, Procedia Eng. 57 (2013) 99–106, https://doi.org/10.1016/j.proeng.2013.04.015.
[47] M.C. Alonso, J. Vera-Agullo, L. Guerreiro, V. Flor-Laguna, M. Sanchez, M. Collares-Pereira, Calcium aluminate based cement for concrete to be used as thermal energy

storage in solar thermal electricity plants, Cement Concr. Res. 82 (2016) 74–86, https://doi.org/10.1016/J.CEMCONRES.2015.12.013, 82 (2016) 74–86.
[48] J. Puig Montraveta, F. Sánchez Pírez, Los cementos aluminosos y sus aplicaciones refractarias, Bol. Soc. Espanola Ceram. Vidr. 13 (1974) 19–24.
[49] E.C. Dapples, W.C. Krumbein, L.L. Sloss, Petrographic and lithologic attributes of sandstones, J. Geol. 61 (1953) 291–317, https://doi.org/10.1086/626098.
[50] M.C. Powers, A new roundness scale for sedimentary particles, J. Sediment. Res. 23 (1953) 117–119, https://doi.org/10.1306/D4269567-2B26-11D7-8648000102C1865D.
[51] E. John, M. Hale, P. Selvam, Concrete as a thermal energy storage medium for thermocline solar energy storage systems, Sol. Energy 96 (2013) 194–204, https://doi.org/10.1016/j.solener.2013.06.033.
[52] R. Tiskatine, A. Eddemani, L. Gourdo, B. Abnay, A. Ihlal, A. Aharoune, L. Bouirden, Experimental evaluation of thermo-mechanical performances of candidate rocks for use in high temperature thermal storage, Appl. Energy 171 (2016) 243–255, https://doi.org/10.1016/j.apenergy.2016.03.061.
[53] U. Diederichs, M.C. Alonso, U.M. Jumppanen, Concerning effects of moisture content and external loading on deterioration of high strength concrete exposed to high temperature, in: Proceedings 1st International Workshop on Concrete Spalling Due to Fire Exposure, 2009. Leipzig, Germany.
[54] W. Khaliq, H.A. Khan, High temperature material properties of calcium aluminate cement concrete, Constr. Build. Mater. 94 (2015) 475–487, https://doi.org/10.1016/j.conbuildmat.2015.07.023.
[55] UNE EN 1992-1-1:2013 Eurocode 2: Design of Concrete Structures - Part 1-1, General rules and rules for buildings, 2013.